Enhanced visible light-triggered antibacterial activity of carbon quantum dots/polyurethane nanocomposites by gamma rays induced pre-treatment

Milica Budimir, Zoran Markovic, Jan Vajdak, Svetlana Jovanović, Pavel Kubát, Petr Humpoliček, Matej Mičušík, Martin Danko, Alexandre Barras, Dušan Milivojević, et al.

Version of Record: https://www.sciencedirect.com/science/article/pii/S0969806X21001493
Manuscript_1ebd31a9d7bffb83b45b5c0812a2e60c

Enhanced visible light-triggered antibacterial activity of carbon quantum dots/polyurethane nanocomposites by gamma rays induced pre-treatment

Milica Budimir[1,2,3], Zoran Marković[2], Jan Vajdak[4], Svetlana Jovanović[2], Pavel Kubat[6], Petr Humpoličeк[4], Matej Mičušik[5], Martin Danko[5], Alexandre Barras[3], Dušan Milivojević[2], Zdenko Špitalsky[5], Rabah Boukherroub[3], Biljana Todorović Marković[2]

[1]*School of Electrical Engineering, University of Belgrade, Bulevar kralja Aleksandra 73, 11000 Belgrade, Serbia*

[2]*Department of Radiation chemistry and physics, „VINČA" Institute of Nuclear Sciences - National Institute of the Republic of Serbia*

[3]*Univ. Lille, CNRS, Centrale Lille, Univ. Polytechnique Hauts-de-France, UMR 8520 - IEMN, F-59000 Lille, France*

[4] *Centre of Polymer Systems, Tomas Bata University in Zlin, Trida Tomase Bati 5678, Zlin, Czech Republic*

[5]*Polymer Institute, Slovak Academy of Sciences, Dúbravská cestá 9, 84541 Bratislava, Slovakia*

[6] *J. Heyrovsky Institute of Physical Chemistry, Academy of Sciences of the Czech Republic, Dolejškova 3, 182 23 Praha 8, Czech Republic*

Corresponding author

Milica Budimir, e-mail: budimir@vin.bg.ac.rs address: Mike Petrovića Alasa 12-14, 11001 Belgrade, Serbia.

Abstract

Persistent microbial contamination of medical implant surfaces is becoming a serious threat to public health. This is principally due to antibiotic-resistant bacterial strains and the formation of bacterial biofilms. The development of novel antibacterial materials that will effectively fight both Gram-positive and Gram-negative bacteria and prevent biofilm formation represents a big challenge for researchers in the last few decades. In the present work, we report an antibacterial hydrophobic carbon quantum dots/polyurethane nanocomposite (hCQD-PU), with enhanced antibacterial properties induced by pre-treatment with gamma-irradiation. Hydrophobic quantum dots (hCQDs), which are capable of generating reactive oxygen species (ROS) upon irradiation with low-power blue light (470 nm), have been integrated into the polyurethane (PU) polymer matrix to form a photoactive nanocomposite. To modify its physical and chemical properties and improve its antibacterial efficacy, various doses of gamma irradiation (1, 10, and 200 kGy) in the air environment were applied to the formed nanocomposite. Gamma-irradiation pre-treatment significantly influenced the rise in ROS production, therefore, the prooxidative activity under the blue-light illumination of hCQD-PU was also significantly improved. The best antibacterial activity was demonstrated by the hCQD-PU nanocomposite irradiated with a dose of 200 kGy, with the complete eradication of Gram-positive *Staphylococcus aureus (S. aureus)* and Gram-negative *Escherichia coli (E. coli)* bacteria after 15 min of exposure to the blue lamp.

Keywords: *Polymer-matrix composite; Carbon quantum dots; Gamma-irradiation; Reactive oxygen species, Antibacterial photodynamic therapy.*

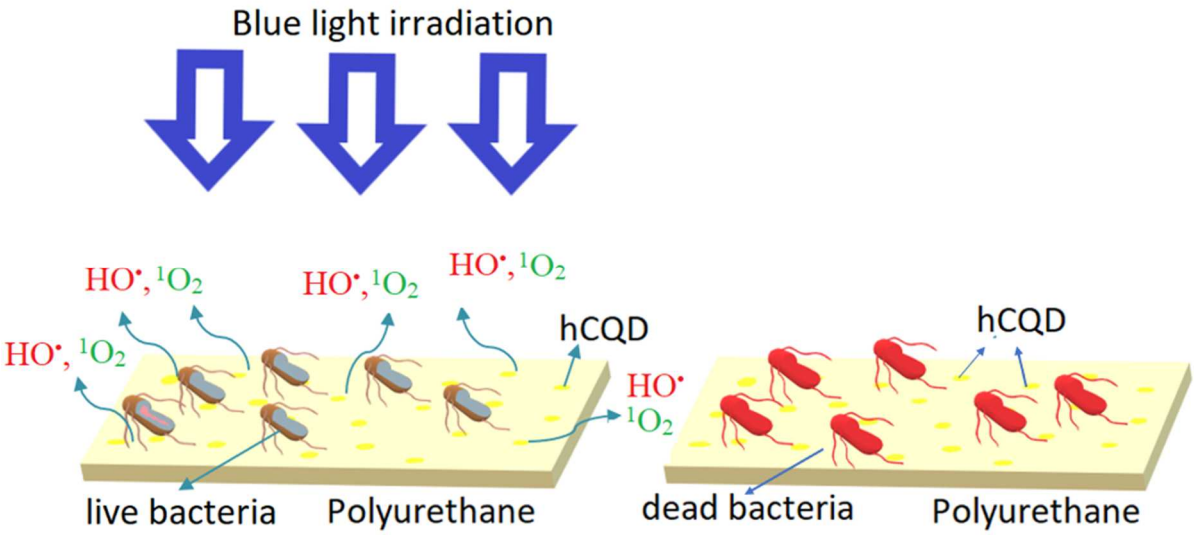

1. Introduction

Antimicrobial resistance is a medical issue that represents a serious threat to global public health [1]. The misuse of antibiotics has led to the development of multi-resistant pathogenic strains [2], which further led to the inefficacy of many traditional therapies. It is now well understood that bacteria survive by attaching to solid surfaces, where they start creating a self-produced matrix of extracellular polymeric substances. This matrix forms the foundation of a biofilm, which provides a protective environment for microbial pathogens [3]. Bacteria in biofilms are drastically more resistant to antibiotics, external forces and host defense mechanisms. Nosocomial infections (hospital-acquired) are primarily caused by bacterial colonization of a wide range of biomedical surfaces. The prevalence rate of nosocomial infections ranges from 4% to 10% (reaching up to 30% in intensive care units) in western-industrialized countries, making them the sixth-leading cause of death [4–6]. The proportion is even higher (>15%) in developing countries [7]. The formation of a biofilm on a biomedical device for implantation can be very dangerous, leading to many post-surgical complications such as infections, implant rejection, and even death [1,8,9]. Also, the surfaces in the near-patient environment play a major role in the spread of nosocomial infections [5]. Therefore, the development of antibacterial surfaces and coatings, that will prevent the bacterial colonization of biomedical surfaces is the key to limiting and eliminating nosocomial infections. However, this is a very challenging task because many factors influence bacteria adhesion and attachment, such as surface properties (roughness, wettability, surface charge), characteristics of the aqueous medium, and types of microorganisms [10,11].

Some classifications suggest that antibacterial surfaces can be divided into two categories, anti-biofouling and bactericidal [8]. A surface that is capable of repelling or limiting microbial attachment is considered “anti-biofouling”. On the contrary, “bactericidal surface” allows the attachment of microbes but has a mechanism to disrupt the attached cells, which results in cell death. Bactericidal surfaces can either chemically or physically disrupt the cell morphology, or by combining both mechanisms [9]. The chemical approach means that the surface is chemically modified, functionalized, or coated with biocidal material (nanoparticles [12–15], polymers [16–18], antibiotics [19,20]), while the physical approach includes different methods to modify the topography of the material, in order to kill the microbes.

Nanoparticles have demonstrated excellent antimicrobial activity towards a broad spectrum of Gram-negative, Gram-positive bacteria [9,21–24] and fungi [25]. Consequently,

their incorporation in carrier matrixes (usually polymers) to form antibacterial nanocomposites, have been widely considered in both the biomedical field and water purification systems. Nanomaterials derived from silver [26–28], gold [29,30], zinc oxide [31], calcium oxide [23], titanium dioxide [32,33], magnesium oxide [34], copper oxide [35] and graphene-based nanomaterials [36] have been researched as efficient coatings, wound dressings, and in cosmetics and food storage applications [37]. However, certain nanoparticles need to be triggered by the UV light (TiO_2, ZnO), while some can produce ROS already at the ambient light (Ag NPs, CuO, MgO, CaO). There are many different toxicity mechanisms [24] among nanoparticles, and microbes are not likely to grow resistance against them. However, several studies have revealed that metal nanomaterials induce acute tissue toxicity in humans, which has resulted in their limited use [38].

Carbon quantum dots (CQDs) are a class of 0-dimensional nanocarbons, consisting of quasi-spherical nanoparticles with sizes below 10 nm and exceptional properties [39,40]. Their main characteristics are excellent chemical stability, water-dispersibility, ease of functionalization, multicolor emission in the visible region, and photobleaching resistance [41]. They are also a very efficient photosensitizer (PS) capable of producing reactive oxygen species (ROS) upon photo-excitation, which, combined with high biocompatibility [39,42–44], makes them excellent agents for photodynamic therapy [41,45].

When PS reacts with molecular oxygen, ROS are formed via one of the two mechanisms: Type I and Type II. Type I mechanism produces superoxide ($O_2^{\bullet-}$), hydroxyl radical ($^{\bullet}OH$), and hydrogen peroxide (H_2O_2), and Type II mechanism results in the production of singlet oxygen ($^1O_2$) [46]. Generated ROS ($^{\bullet}OH$, $O_2^{-\bullet}$, H_2O_2, $^1O_2$) can cause oxidative stress on the cell membrane, by attacking lipids and proteins, thus leading to cell membrane destruction. Researchers have conducted many experiments to determine if CQDs undergo both Type I and Type II photosensitization mechanisms [47]. Nie et al. [48] explored the production of all four types of ROS to determine the mechanism of antibacterial action of CQDs. Their results showed that only singlet oxygen was detected, meaning that the CQDs were operating via Type II mechanism. Singlet oxygen detection was also confirmed in hydrophobic carbon quantum dots by Stankovic et al. [49], and in brominated carbon nanodots by Knoblauch et al. [50]. On the contrary, some other studies [51] reported the presence of Type I or even multiple Type I [52] mechanisms, while a study by Zhang et al. [53] reported the formation of both $O_2^{\bullet-}$ (Type I), and ($^1O_2$) (Type II).

Polyurethane (PU) is widely used in healthcare applications and a variety of medical devices, such as potting material in artificial dialysis devices, plasma separators, catheters,

etc. [54]. In the sterilization process of PU, gamma-irradiation, autoclave, and different chemical agents are currently employed.

High-energy treatment of polymers, such as gamma-irradiation, can result in free radicals generation, chain scission, and crosslinking, and subsequently alters the chain size in the bulk polymer [56–61]. The effect of the gamma irradiation on the physical and chemical properties of a polymer depends on the irradiation medium, dose rate, polymer's properties, etc. In the work of Cooke et al. [62] when polyurethane was irradiated in the air at 25 kGy but at different dose rates (0.192 kGy h^{-1}, and 49.98 kGy h^{-1}), gamma-irradiation did not induce any structural, morphological, or mechanical changes in polyurethane. However, irradiation at higher doses, up to 100 kGy, caused chain scission and crosslinking [54]. Another study confirmed that irradiation of polyurethane in air leads to polymer crosslinking, at a high irradiation dose (150 kGy) [63]. Due to this feature, gamma-irradiation is often used for improving the strength and abrasion resistance of polyurethane [58].

The application of gamma irradiation as a pre-treatment method in the present research was motivated by the encouraging results obtained previously in our group [64,65], where the most interesting finding was an improved singlet oxygen generation ability of graphene quantum dots, after the gamma-irradiation pre-treatment [64], and improved photoluminescent properties of the gamma-irradiated polyurethane/carbon quantum dots nanocomposites [65].

In this work, we present a nanocomposite that consists of a polymer (polyurethane - PU) with incorporated hydrophobic carbon quantum dots (hCQDs) inside its matrix, which exhibits antibacterial properties when irradiated by blue light. Here, our goal was to improve the antibacterial properties of hCQD-PU nanocomposite [66] by gamma-irradiation pre-treatment. The advantage of this material is the resistance to photo-bleaching and the fact that hCQD can be triggered by visible light, unlike many other photosensitizers. As targets, we used *S. aureus,* a Gram-positive bacterium causing serious healthcare-associated infections, and *E. coli*, a Gram-negative pathogenic strain, which is responsible for urinary and gastrointestinal tract infections.

2. Experimental

2.1 Materials

Commercially available medical grade transparent PU with a thickness of 1mm, was donated by American Polyfilm (Aliphatic TPU film). Polyoxyethylene-polyoxypropylene-

polyoxyethylene Pluronic 68 was obtained from Interchim (France). Phosphoric acid and toluene were purchased from Sigma Aldrich, Germany, and used as received.

2.2 Preparation of hydrophobic carbon quantum dots/polyurethane nanocomposite (hCQD-PU)

The synthesis of hydrophobic carbon quantum dots (hCQDs) was performed according to the previously described method [49,66]. Firstly, 1g of polyoxyethylene-polyoxypropylene-polyoxyethylene Pluronic 68 was dissolved in 100 mL of water, in an ultrasonic water bath. Then, phosphoric acid was added (200 mL) and the mixture was stirred, in order to become homogeneous. While stirring, the temperature of the magnetic stirrer was slowly increased, until it reached 250 °C and after 145 min, the solution became brown. Then, the mixture was left to cool down to room temperature, and 250 mL of water was added. The mixture was again stirred for another 2 h, without heating, until a brownish-black colored precipitate was obtained. Finally, 300 mL of toluene was added to the solution. The reaction mixture was stirred overnight at room temperature until the solution turned yellow. Finally, the organic phase was decanted and then filtered using a vacuum pump, through hydrophobic membrane filters with pore sizes of 0.2 and 0.1 μm. The obtained product was a colloid of hCQDs.

PU film was cut first into stripes which were 2.5 cm wide and around 20 cm long, and they were immersed into the solution of hCQDs (1 mg mL^{-1}) in toluene in a graduated cylinder, for 48 h. The obtained hCQD-PU nanocomposite was dried in the vacuum furnace for 12 h at 80°C, to evaporate all the remaining toluene. The hCQDs were incorporated inside of the polymer matrix by the swell-encapsulation-shrink method [16]. Then, both the pure PU and the hCQD-PU nanocomposite samples were exposed to the gamma irradiation at 1, 10 and 200 kGy doses (throughout the manuscript samples are labeled as $_{1}\gamma$-PU, $_{10}\gamma$-PU, $_{200}\gamma$-PU, $_{1}\gamma$-hCQD-PU, $_{10}\gamma$-hCQD-PU, and $_{200}\gamma$-hCQD-PU) [65]. Gamma-irradiated pure polyurethane samples served as control.

The samples were irradiated in the air atmosphere by gamma-ray flux from ^{60}Co nuclide with the photon energy of 1.3 MeV (Centre of Irradiation, Vinca Institute of Nuclear Sciences) at a dose rate of 13 kGy h^{-1}.

2.3 Characterization of the hCQDs and hCQD-PU nanocomposites

X-photoelectron spectroscopy (XPS) was used to determine the chemical composition of the gamma-irradiated hCQD-PU nanocomposites. The measurements were performed on a Thermo Scientific K-Alpha XPS system using monochromatic Al Kα X-ray source.

The wetting properties and morphology of the nanocomposites were assessed using contact angle and atomic force microscopy measurements, respectively. The contact angles of the γ-irradiated hCQD-PU nanocomposites were measured by the Surface Energy Evaluation System (SEE System; Advex Instruments, Czech Republic), and the software from this system has been used for further analysis. To measure the contact angle, 2 μL of deionized water was used. All measurements were performed in the ambient atmosphere, at room temperature, and in triplicates.

Atomic force microscopy (AFM) was used to visualize the surface morphology of the gamma-irradiated hCQD-PU. Measurements were acquired using a Quesant microscope (Ambios Technology, USA), and its software. The AFM measurements were performed using a silicone T-shaped cantilever with a spring constant of 40 N/m, in air and at room temperature. The surface was scanned over different square areas at 512 × 512 image resolution. To determine the root-mean-square roughness (RMS) values of hCQD-PU nanocomposites, Gwyddion software was used [67].

2.4 Reactive oxygen species (ROS) determination

2.4.1 Quenching of free radicals

To investigate radical scavenging activity (RSA) of the nanocomposites, the DPPH assay was used [68]. This experiment is based on the characteristic of the molecule 2,2-diphenyl-1-picrylhydrazyl (DPPH) to show strong UV-vis spectrum absorption at 518 nm. In this form, DPPH is a stable free radical. In the presence of antioxidants, DPPH forms a yellow compound which can be observed by UV-vis as a reduction in the band intensity at 518 nm. To quantify the RSA value, a fresh solution of DPPH (100 μM in methanol) was prepared and the different sizes of PU, gamma-irradiated PU, and hCQD-PU nanocomposites (0.5×0.5, 1.0×1.0, 1.5×1.5 cm^2) were dipped into the solution. The samples were incubated in dark with DPPH solution for 1 h, and the absorbance of the solution was measured at 518 nm using a GBC Cintra 6 Spectrophotometer (GBC Dandenong, Australia). As a control, a methanol solution of ascorbic acid was used. For each sample, the RSA values were calculated using the formula RSA (%) = $(Ac-A_{PU-CQDs})/Ac \times 100$, where Ac is the intensity of

absorption of control (DPPH in methanol) and A_{PU-CQD} is the intensity of the absorption band of a solution in which samples were dipped. Measurements were replicated three times.

Additionally, we investigated the ability of composites to adsorb DPPH. To avoid false-positive radical scavenging activity, which can be caused by physical adsorption of DPPH molecules by hCQD-PU, we soaked the composites (1.5 x 1.5 cm2) into DPPH methanol solution (100 μM) and after 1 h of incubation in dark, we recorded absorption spectra of composites (without previous rinsing).

2.4.2 Singlet oxygen production and oxygen lifetime measurements

A piece of hCQD-PU nanocomposite was inserted into a quartz cell in an oxygen or air atmosphere. For measurements in oxygen-free conditions, the samples were evacuated for at least 15 min. The total pressure in the cell was measured with capacitance manometers (MKS Baratron).

Following the excitation of individual samples using COMPEX 102 excimer laser (wavelength 308 nm, pulse width ~28 ns), the kinetics of singlet oxygen, $O_2(^1\Delta_g)$ was measured using time-resolved near-infrared luminescence spectroscopy. Luminescence of $O_2(^1\Delta_g)$ at 1270 nm was recorded in reflection mode using a Judson Ge diode and interference filters.

The signal from the detector was collected in a 600 MHz oscilloscope (Agilent Infiniium) and forwarded to a computer for further analysis. Averaging 1000 individual traces increased the signal-to-noise ratio of the signals. The initial part (up to 2 μs) was not used for assessment due to a large scattering of the laser pulse and luminescence of hCQDs and other compounds.

The transient absorption spectra in the visible part of spectra (400-720 nm) and kinetics of transients at 520 nm were recorded with a 150 W Xe lamp (Phillips) equipped with a pulse unit and R928 photomultiplier (Hamamatsu) using a laser kinetic spectrometer LKS 20 (Applied Photophysics, UK).

2.4.3 Production of hydroxyl radicals (•OH)

The formation of •OH radicals on the sample surface under UV excitation was studied by fluorescence technique on a Hitachi F-4500 fluorescence spectrophotometer. Terephthalic acid was used as it interacts easily with •OH radicals, creating a strongly fluorescent product, 2-hydroxyterephthalic acid, which exhibits a peak at the wavelength of about 425 nm at the excitation of 315 nm. It was established that the peak strength assigned to the 2-

hydroxyterephthalic acid was proportional to the amount of •OH radicals produced [69]. The concentration of the terephthalic acid solution was 5×10^{-4} M in a diluted NaOH aqueous solution with a concentration of 2×10^{-3} M. It has been proved that under these experimental conditions (concentration of terephthalic acid < 10^{-3} M, room temperature), the hydroxylation reaction of terephthalic acid proceeds mainly by •OH radicals [69].

Gamma-irradiated hCQD-PU samples were added to 200 mL of the 5×10^{-4} M terephthalic acid solution in 2×10^{-3} M NaOH and then exposed to the blue light (470 nm), with the power of the lamp of 15 W. Sampling was performed every 15 min, and the solution was analyzed after filtration through 0.45 μm membrane filter.

2.4.4 Electron Paramagnetic Resonance (EPR)

Electron Paramagnetic Resonance (EPR) analyses were performed using a Spectrometer MiniScope 300, Magnettech, Berlin, Germany. Measurements were performed at room temperature. The microwave power was 1 mW (microwave attenuation of 20 dB), with a modulation amplitude of 0.2 mT. The instrument was operating at a nominal frequency of 9.5 GHz. The samples were cut into 0.5 mm strips and inserted into a narrow tube where it was mixed with an ethanol solution of DMPO and exposed to UV light. The concentration of DMPO was 15 mM.

The production of hydroxyl (•OH), superoxide ($O_2^{-\bullet}$), and alkyl ($CH_3^{\bullet}$) radicals was investigated using 5,5-dimethyl-1-pyrroline-N-oxide (DMPO) as a spin trap. The molecules of DMPO react with radicals to form stable spin adducts, radical products with distinct EPR spectra. These reactions allow following the production of these radical species. The samples were cut into 0.5 mm strips and inserted into a narrow tube where it was mixed with an ethanol solution of DMPO and exposed to UV light. The concentration of DMPO was 15 mM.

2.5 Bacteria culture and preparation for antibacterial testing

The bacteria used in this study were *S. aureus* CCM 4516 (Gram-positive) and *E. coli* CCM 4517 (Gram-negative) pathogenic strains. The bacterial strains were purchased from CCM (Czech Collection of Microorganisms). Antibacterial activity was carried out following ISO 22196 standard – Measurement of antibacterial activity on plastics and other non-porous surfaces [70]. The dimensions of the tested samples were 2.5 × 2.5 cm. Blue light (470 nm)

was used to trigger hCQDs, the power of the lamp was 15 W, and the distance between samples and the lamp was 50 cm. The tested samples were irradiated for 15 and 5 min.

2.6 Biocompatibility studies

2.6.1 Cytotoxicity study of released extracts

Cytotoxicity of extracts, prepared in the presence of gamma-pretreated hCQD-PU nanocomposites, was determined. Before the experiments, samples (1×1 cm^2) were sterilized in ethanol and dried. Sterilized samples were then incubated in 1 mL of Dulbecco's Modified Eagle's medium (DMEM, Gibco®) supplemented with 10% fetal bovine serum (FBS, Gibco®) and 1% penicillin-streptomycin (Gibco®) during 24 h at 37 °C and 5% CO_2. The released medium was after incubation diluted with fresh medium at different concentrations (from 1% to 100%) and tested in contact with cells for 24 h. U-87 MG derived from a malignant glioma from a female patient by explant technique [ECACC 89081402, Sigma Aldrich, Saint-Quentin Fallavier, France] and HeLa cell line derived from cervical carcinoma from a 31-year-old female [ECACC 93021013, Sigma Aldrich, Saint-Quentin Fallavier, France] were used as model cell lines. Cells were maintained in DMEM supplemented with 10% FBS and 1% penicillin-streptomycin in a humidified incubator at 37 °C and 5% CO_2. Briefly, cells were seeded at a density of 10^4 cells/well in a 96-well plate for 24 h before assay. The culture medium was then replaced with extracts. After 24 h, cells were washed with PBS and the cell viability was evaluated using resazurin cell viability assay. 100 mL of the resazurin solution (11 µg mL^{-1}) in DMEM/10% FBS were added to each well and the plate was incubated for 4 h in the humidified incubator. A Cytation™ 5 Cell Imaging Multi-Mode Reader was used to measure the fluorescence emission of each well at 593 nm (20-nm bandwidth) with an excitation at 554 nm (18-nm bandwidth). Each condition was replicated three times and the mean fluorescence value of non-exposed cells was taken as 100% cellular viability.

2.6.2 Cell proliferation and growth

U-87 MG [ECACC 89081402, Sigma Aldrich, Saint-Quentin Fallavier, France] and HeLa cell line [ECACC 93021013, Sigma Aldrich, Saint-Quentin Fallavier, France] were maintained in DMEM supplemented with 10% FBS and 1% penicillin-streptomycin in a humidified incubator at 37 °C and 5% CO_2.

Determination of cell morphology: Determination of cell morphology was performed by Hoechst 33258 (Invitrogen, USA) for staining the DNA. First, the volume of 100 µL of a

concentration of 80000 cells mL^{-1} was seeded directly onto samples, and after 1 h, 1 mL of complete culture medium was added. It was cultivated for 48 h. Cells were then fixed, stained, and finally observed by fluorescence microscopy.

Cell fixation: To fix cells, 4% paraformaldehyde (PFA) was added to cells for 15 min. After the cells were washed 3 times by PBS (Invitrogen, USA), 1 mL of PBS containing Hoechst 33258 (5 µg/mL) was added to samples and left to incubate in the dark. After 10 min, cells were washed again and ready for microscopic observation.

Microscopic observation: Fluorescence images (DAPI exc. 377/50 nm and em. 447/60 nm) were captured using a Cytation™ 5 Cell Imaging Multi-Mode Reader (BioTek Instruments SAS, France) and analyzed by Gen5iPlus 3.04 Imaging Software.

3 Results and discussion

Gamma irradiation induces changes in both polymer and carbon quantum dots, and both effects will be discussed in the following sections. After gamma-pretreatment of PU and hCQD-PU, a noticeable color change occurred. Firstly, polyurethane was colorless, and after the incorporation of hCQDs in the PU matrix, it became light yellow (**Fig. S1**). Also, after gamma-irradiation the color of both PU and hCQD-PU became light yellow, gradually turning darker yellow with the increase of the irradiation dose. The discoloration is a common change in the irradiation processing of polymers [71]. As discussed in many papers [71–73], there are two types of radiation-induced color centers in polymeric materials: annealable and permanent. It is considered that the annealable centers are connected with free radicals trapped inside the polymer matrix, while permanent color centers lead to the formation of stable conjugated chromophores within the polymer [71].

3.1 X-ray photoelectron spectroscopy (XPS)

The XPS was used to characterize the elemental composition of gamma-irradiated hCQD-PU nanocomposites, and the XPS wide scan displayed that these nanocomposites were composed of the elements: C, O, and N (**Table 1**). The content of the characteristic bonds in $_{1}\gamma$-hCQD-PU, $_{10}\gamma$-hCQD-PU, and $_{200}\gamma$-hCQD-PU were detected and compared by fitting C1s (**Table 2**).

The XPS analysis results demonstrated that the percentage of sp^3 bonds decreased with the increase of the dose of gamma irradiation, while consequently, the percentage of sp^2 bonds increased (**Table 2**). This indicates the more arranged structure of hCQD inside of the PU

matrix in the $_{200}$γ-hCQD-PU sample [74]. Additionally, the content of oxygen was almost doubled in the sample $_{200}$γ-hCQD-PU, compared to the $_{10}$γ-hCQD-PU sample (**Table 1**), while the content of nitrogen decreased with the increase of the gamma-irradiation dose. After irradiation at a dose of 1 kGy, the N content increased to 5.8 at. %, while at higher doses the nitrogen content in the structure of composite was lowered to 4.7 and 4.1 at. %. Gamma irradiation in the air as a medium, leads to the incorporation of N functional groups in carbon-based nanomaterials [75], while at a dose of 10 to 100 kGy, C-N bonds on the amide functional groups can be broken into an ester (O=C-O) groups [76]. Due to this change, the content of N is lowered for samples irradiated at doses of 10 and 200 kGy.

From the results presented in **Table 2**, we can also conclude that the content of oxygenated bonds was the lowest for the $_{10}$γ-hCQD-PU sample and the highest for the $_{200}$γ-hCQD-PU sample [65]. This is probably due to the reaction of free radicals produced upon radiolysis with oxygen, which was larger at the higher radiation dose [77,78].

Table 1. Elemental composition of gamma-irradiated hCQD-PU samples.

Name	**hCQD-PU** [66]	**$_{1}$γ-hCQD-PU (at. %)**	**$_{10}$γ-hCQD-PU (at. %)**	**$_{200}$γ-hCQD-PU (at. %)**
N1s	3.3 ± 0.1	5.8 ± 0.1	4.7 ± 0.1	4.1 ± 0.1
C1s	80.1 ± 0.1	85.2 ± 0.1	90.4 ± 0.1	87.1 ± 0.1
O1s	13.1 ± 0.1	6.5 ± 0.1	4.8 ± 0.1	8.7 ± 0.1

Table 2. C1s deconvolution of gamma-irradiated hCQD-PU samples.

Name	**hCQD-PU** [66]	**$_{1}$γ-hCQD-PU (at. %)**	**$_{10}$γ-hCQD-PU (at. %)**	**$_{200}$γ-hCQD-PU (at. %)**
sp^2	27.9 ± 0.1	28.9 ± 0.1	39.9 ± 0.1	49.2 ± 0.1
sp^3	49.3 ± 0.1	55.2 ± 0.1	50.1 ± 0.1	32.8 ± 0.1

C-O	13.9 ± 0.1	10.2 ± 0.1	4.4 ± 0.1	13 ± 0.1
C = O	4.5 ± 0.1	0.5 ± 0.1	0	0
O-C=O	1.2 ± 0.1	1.2 ± 0.1	0	0.7 ± 0.1
N-C=O	3.2 ± 0.1	4.0 ± 0.1	5.6 ± 0.1	4.4 ± 0.1

*Standard deviation for all XPS measurements is 0.1 [79]

3.2 Wetting properties

Measurements of the water contact angle (WCA) were carried out to investigate the hydrophobicity/hydrophilicity of the samples. The results revealed that the contact angle decreased as the gamma irradiation dose increased, compared to the contact angle before gamma pretreatment [65] (**Table 3**). Decreasing the contact angle is advantageous as it can enhance bacterial cell adhesion. Some study findings have shown that the adhesion is optimum when the contact angle is around 70°, whereas higher and lower contact angles decrease bacteria adhesion [80,81]. Contact angle variations may be a consequence of different chemical composition or surface structure [82], and both effects are present in our samples, meaning that after gamma-irradiation the surface roughness of hCQD-PU has changed (which will be discussed in the next paragraph), but also the elemental composition of the sample (which was shown as XPS results).

Table 3. Surface roughness and contact angle.

Sample	**Contact angle (°)**	**RMS roughness (nm)**
hCQD-PU	112 ± 2	18 ± 1
$_{1}\gamma$-hCQD-PU	96 ± 2	21 ± 1
$_{10}\gamma$-hCQD-PU	84 ± 2	36 ± 1
$_{200}\gamma$-hCQD-PU	73 ± 2	62 ± 1

3.3 Atomic force microscopy (AFM)

The morphology and surface roughness of gamma-irradiation pre-treated samples were analyzed by AFM. From the AFM images, we can easily detect the difference in the surface morphology of various samples (**Fig. 1**). This was confirmed through the study of each sample's average surface roughness, obtained from several AFM images (**Table 3**). As the dose of gamma irradiation increased, the surface roughness increased significantly. It is not entirely consistent with the measurements of the contact angle, because generally when a hydrophobic material becomes rougher it reaches super-hydrophobicity [73]. However, there was a noteworthy change in the chemical composition of materials after gamma-pretreatment, which also influenced the surface roughness. These results are in accordance with the results of Gorna et al. which also showed the increase of surface roughness after gamma-irradiation of polyurethane samples [83].

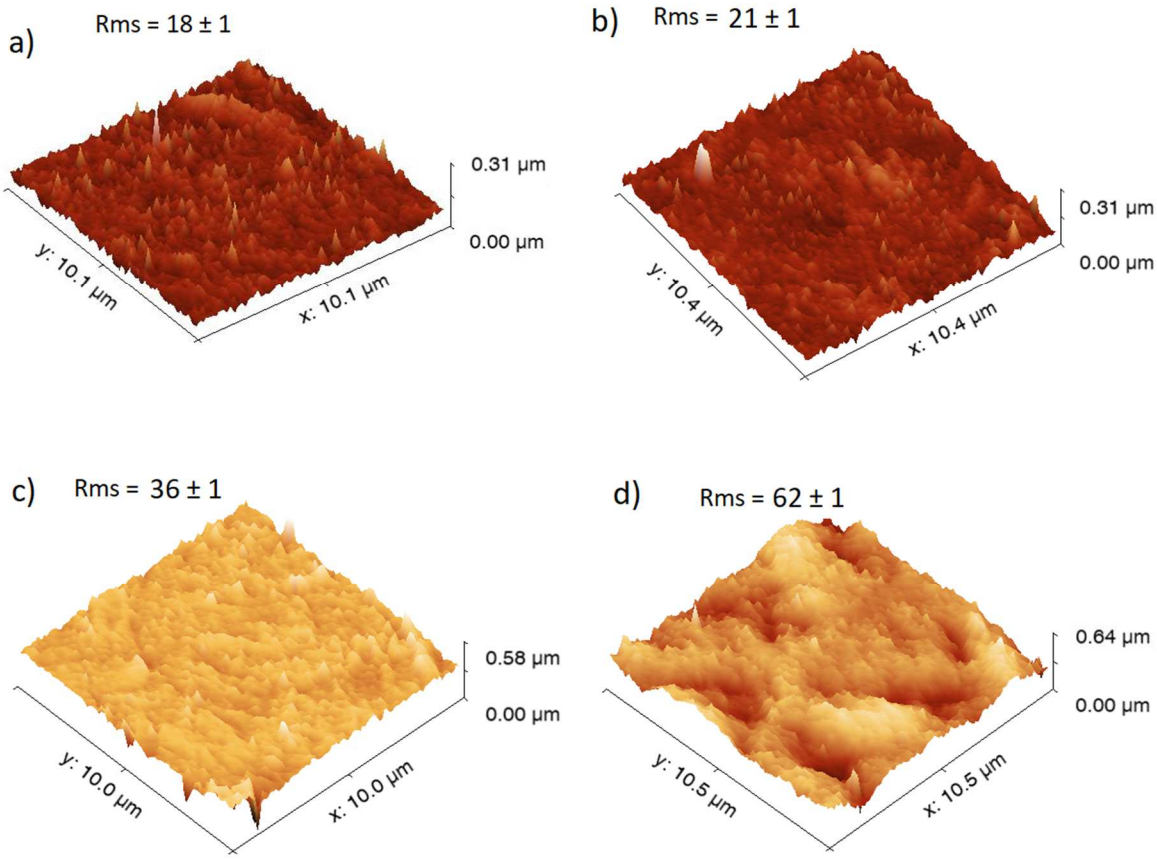

Figure 1. 3D AFM images of hCQD-PU sample before (a) and after gamma pre-treatment: b) $_{1}$γ-hCQD-PU, c) $_{10}$γ-hCQD-PU, and d) $_{200}$γ-hCQD-PU, scan size in each image is 10×10 µm^2.

3.4 DPPH radical scavenging assay

The intensity of the absorption at around 520 nm was measured, after 1 h of incubation of DPPH$^{\bullet}$ with PU, gamma-irradiated PU, and nanocomposites, in the dark, to assess the radical scavenging activity - RSA (**Fig. 2**). As we can see, the intensity of the DPPH band is lowered after incubation with bare and gamma-irradiated PU as well as nanocomposites. As the size of the samples increases, the intensity of the band at 520 nm decreases. The lowest observed intensity is when the size of both polymers and the nanocomposites was the highest (1.5×1.5 cm^2). Thus, it can be concluded that the intensity of the DPPH absorption band is lowering with the increase of the size of the nanocomposites.

DPPH assay indicated that pure PU itself possesses an ability to quench DPPH radicals (**Fig. 2a**). This property of PU was previously detected using also DPPH assay [84]. After gamma irradiation at low doses, of 1 and 10 kGy, the radical quenching ability of PU was not changed largely (**Fig. 2 b, c, and d**). But, the irradiation of polymer at a dose of 200 kGy caused the lowering of its ability to quench DPPH radical. The antioxidative activity of materials depends on their ability to donate the electrons to free radicals. In the case of polymers, phenolic antioxidants or hindered amine were often added as light stabilizers to prevent UV-mediated oxidation and these molecules might lead to antioxidative activity of polymer [85,86]. Upon a high dose of gamma-irradiation, these molecules were possibly degraded which resulted in the loss of antioxidative activity.

Compared to gamma-irradiated PU with hCQDs, the antioxidative ability was much lower than it was measured for pure polymer and gamma-irradiated pure PU (up to 23.07 for $_{10}\gamma$-hCQD-PU, 90.71% for PU and 60.1 for PU irradiated at 200 kGy of the same size, table 4.). Although our previous research showed that gamma irradiation improves hydrogen donation ability of dots and consequently radical quenching capacity [87], herein gamma-irradiation reduced DPPH quenching ability. The principal lowering of RSA values was detected for $_{10}\gamma$-hCQD-PU nanocomposite (**Fig. 2e**), while the XPS analysis of this sample showed the lowest content of C-O bonds. Thus, the lowering in the radical scavenging activity can be explained by the smallest fraction of aromatic hydroxyl edge sites with H-donating activity [68]. Similar behavior was observed for the other two nanocomposites, where the intensity of the DPPH band is decreasing with the size of nanocomposite dipped in DPPH solution (**Fig. 2e-g).** Given that the antioxidative activity arises from both gamma pre-treated hCQDs and polymer stabilizers at lower doses, increasing the nanocomposite's size leads to a higher amount of both antioxidative agents incorporated inside of the polymer matrix, and

consequently to the enhanced antioxidative activity of the gamma pre-treated hCQD-PU samples.

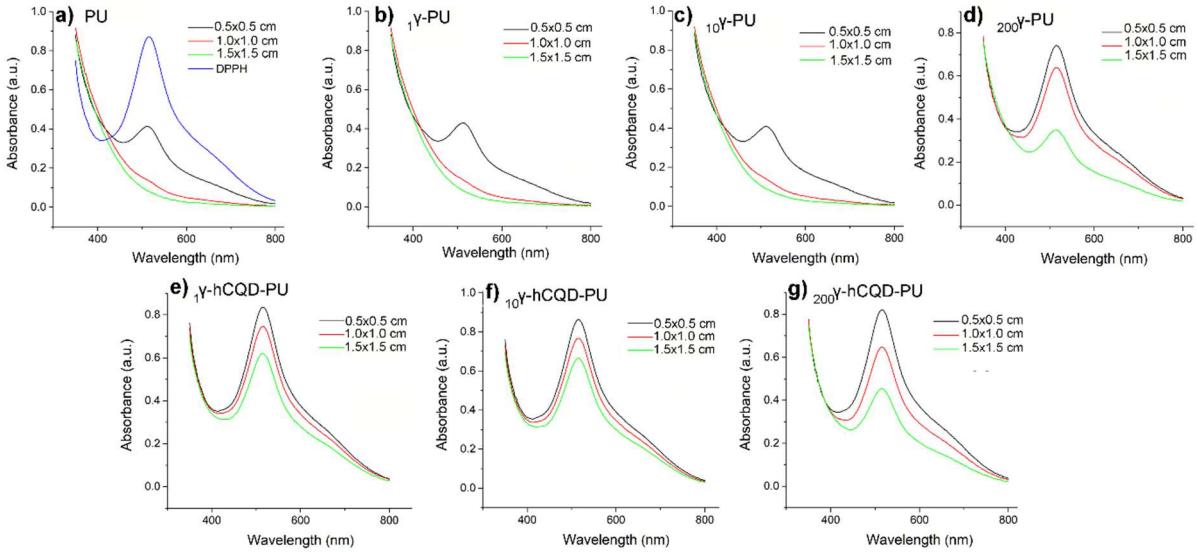

Figure 2. UV-vis spectra of DPPH before and after incubation with different sizes of samples: a) pure PU, b) $_{1}$γ-PU, c) $_{10}$γ-PU, d) $_{200}$γ-PU, e) $_{1}$γ-hCQD-PU, f) $_{10}$γ-hCQD-PU, and g) $_{200}$γ-hCQD-PU.

To exclude any contribution from DPPH adsorption on hCQD-PU composites in the decrease of UV-vis absorption intensity, we measured UV-vis spectra of the nanocomposites after incubation with DPPH for 1h, and all other conditions remained the same (**Fig. 3**). It can be observed that there is no significant absorption at ~520 nm where the main absorption band of DPPH was observed. These results indicate that DPPH adsorption on the hCQD-PU composites is unlikely under our experimental conditions. Thus, it can be concluded that the lowering of this band intensity is due to the conversion of DPPH• into DPPH molecule caused by the antioxidative activity of the nanocomposites.

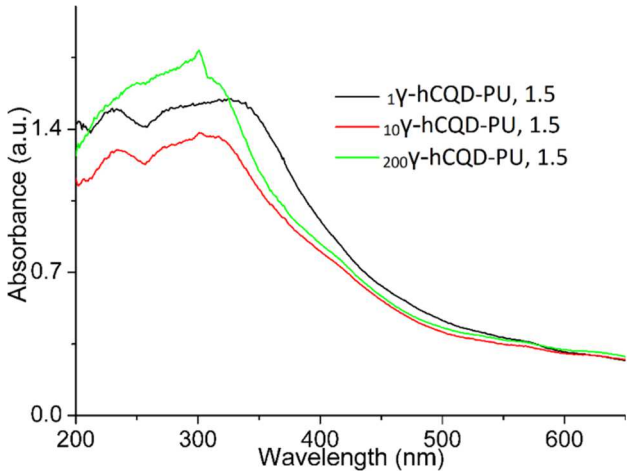

Figure 3. UV-vis spectra of $_{1}$γ-hCQD-PU (black curve), $_{10}$γ-hCQD-PU (red curve), and $_{200}$γ-hCQD-PU (green curve).

Comparing the nanocomposites of the same size, we noticed that $_{200}$γ-hCQD-PU exhibited the highest ability to convert purple DPPH$^{\bullet}$ radicals into a yellow DPPH molecule. This is in accordance with XPS results, which showed that the content of oxygenated bonds was the highest in the $_{200}$γ-hCQD-PU sample and the lowest in the $_{10}$γ-hCQD-PU sample. Calculated RSA values are summarized in **Table 4**.

Table 4. Calculated RSA values for PU, gamma-irradiated PU, and γ-hCQD-PU composites of different sizes.

Sample	Sample size (cm^2)	RSA (%)
PU	0.25	52.98
PU	1	84.40
PU	2.25	90.71
$_{1}$γ-PU	0.25	50.92
$_{1}$γ-PU	1	84.71
$_{1}$γ-PU	2.25	90.71
$_{10}$γ-PU	0.25	53.39
$_{10}$γ-PU	1	84.29
$_{10}$γ-PU	2.25	90.25
$_{200}$γ-PU	0.25	14.91
$_{200}$γ-PU	1	26.72
$_{200}$γ-PU	2.25	60.10
$_{1}$γ-hCQD-PU	0.25	4.2
$_{1}$γ-hCQD-PU	1	14.44
$_{1}$γ-hCQD-PU	2.25	28.90
$_{10}$γ-hCQD-PU	0.25	1.03
$_{10}$γ-hCQD-PU	1	12.04
$_{10}$γ-hCQD-PU	2.25	23.74
$_{200}$γ-hCQD-PU	0.25	5.85
$_{200}$γ-hCQD-PU	1	25.69
$_{200}$γ-hCQD-PU	2.25	48.05

Radical scavenging activity was registered for all nanocomposites. The highest RSA activity was observed for $_{200}$γ-hCQD-PU with a size of 1.5 × 1.5 cm^2. The lowest RSA activity was detected for $_{10}$γ-hCQD-PU (around 23.74 %).

3.5 Singlet oxygen production and lifetime

The broad transient absorption spectra in **Fig. S2a** after excitation correspond to those measured for polyaromatic hydrocarbons [88]. Taking into account the conventional pathway of $O_2(^1\Delta_g)$ formation by energy transfer from the first excited hCQD triplet to the oxygen ground state [89], we searched for transients quenched by oxygen. Our experimental data revealed that the kinetics of transients was complicated and depended on oxygen concentration (**Fig. S2b**). The multiexponential character of the decay kinetics suggests different access pathways of oxygen to the triplet states of hCQD.

To separate the influence of the hCQD triplet states quenched by oxygen that are responsible for the formation of $O_2(^1\Delta_g)$, we calculated the difference between transient absorption in a vacuum and oxygen atmosphere (**Fig. S3b**). The difference in kinetics indicates strong quenching of some triplets by oxygen with lifetime τ_T^{oxy} of a few μs (increasing part of the trace) followed by the decay of the hCQD triplet states, which correspond to the lifetime in a vacuum (τ_T^{vac}) of several hundred μs (decreasing part). Simple calculations show that the fraction F_T of the triplet states trapped by oxygen ($F_T = 1-\tau_T^{oxy}/\tau_T^{vac}$) was very high (> 99%) and indicated the effective formation of $O_2(^1\Delta_g)$. The location of such hCQDs is probably nearby the surface of the film. Note that transients formed by irradiation of pure polyurethane film were not quenched by oxygen (**Fig. S4**).

The formation of $O_2(^1\Delta_g)$ was proved by its characteristic NIR luminescence in the oxygen atmosphere. Due to the very low quantum yield of singlet oxygen (less than 10^{-6}) and increased absorption of hCQD in the UV region, we used excimer laser (308 nm) for excitation to obtain an acceptable signal to noise ratio. At this wavelength, also PU matrix partially absorbed UV radiation and therefore, it was used as a blank sample. The formation of $O_2(^1\Delta_g)$ using direct irradiation of hCQDs by blue light was proven in our previous paper [49] for highly concentrated samples dissolved in chloroform.

All samples pre-treated by γ radiation were compared with original non-irradiated polyurethane film with hCQDs (**Fig. 4**). The values of τ_Δ (singlet oxygen lifetime) were calculated as single-exponential fits to the exponential data after 5 μs after excitation, where

all relevant hCQDs were quenched by oxygen. The calculated lifetimes (τ_Δ ~ 10-11 μs) were not affected by the pretreatment with different doses of γ radiation within estimated experimental error (~10 %), which is due to inhomogeneities of the film. This value is about 3 times longer than that in H_2O (τ_Δ~3.5 μs) [90]. Thus, the polyurethane matrix is "a reservoir" of $O_2(^1\Delta_g)$, from which $O_2(^1\Delta_g)$ gradually releases for a few tens of microseconds to the environment, where it is deactivated quickly by interaction with H_2O or biological targets (bacteria).

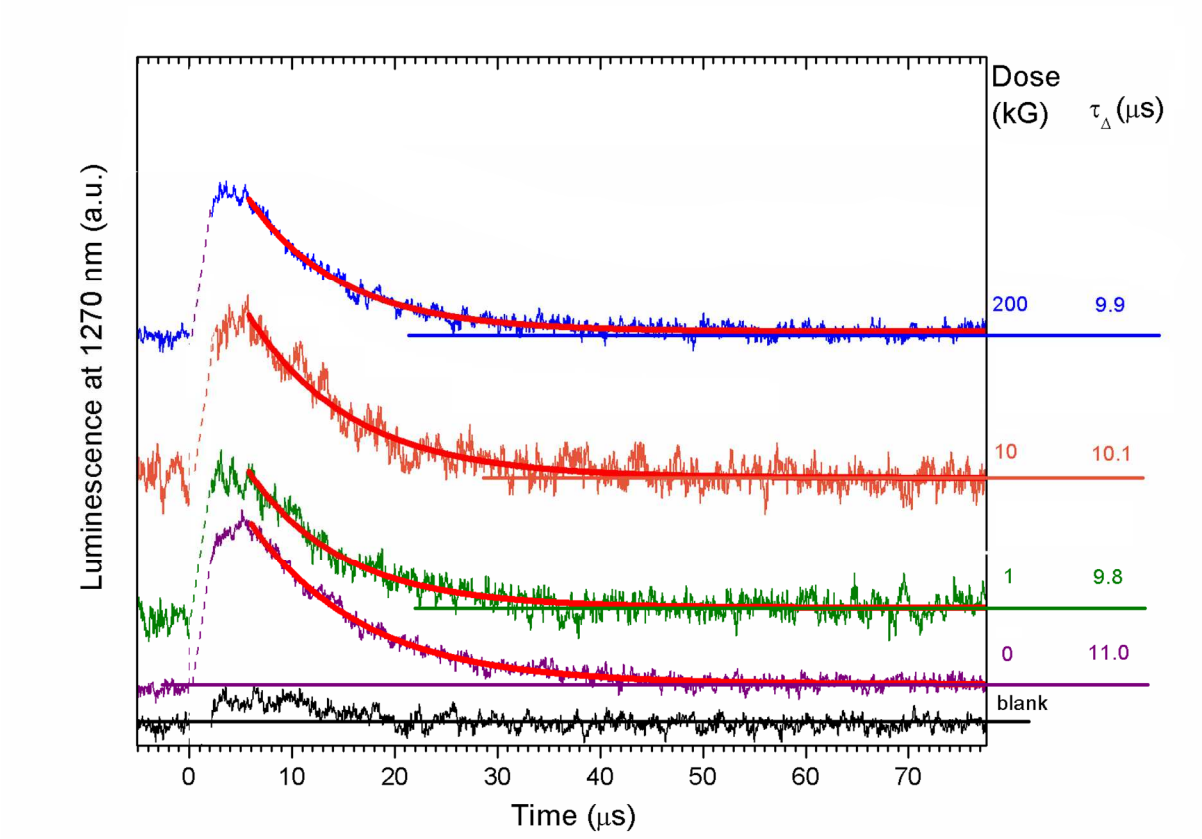

Figure 4. Luminescence of $O_2(^1\Delta_g)$ photogenerated by pulse irradiation of γ-irradiated hCQD-PU nanocomposites, calculated as a difference in an oxygen atmosphere and vacuum. Bare PU (black line); hCQD-PU sample (purple); $_1$γ-hCQD-PU (green); $_{10}$γ-hCQD-PU (orange); $_{200}$γ-hCQD-PU (blue). Data are offset, the region between 0 - 2 μs is omitted due to strong fluorescence and scattering of hCQDs. Red lines are single exponential fits into experimental data with calculated lifetime τ_Δ of $O_2(^1\Delta_g)$.

The diffusion of $O_2(^1\Delta_g)$ photogenerated inside polyurethane film towards bacteria placed in their aqueous environment controls the antibacterial properties. The mean radial diffusion

length of $O_2(^1\Delta_g)$ during time t can be calculated as $l_r = (6\ D(O_2)t)^{1/2}$, where $D(O_2)$ is the oxygen diffusion coefficient. The distance l_r traveled by $O_2(^1\Delta_g)$ during its lifetime, $\tau_\Delta \sim 10$ μs, and for $D(O_2) = 3.2 \times 10^{-7}$ cm^2/cm^2s^{-1} was only 44 nm in the polyurethane film [91]. This value indicates that only hCQDs in the close proximity of polyurethane surface (several tens of nm) can release $O_2(^1\Delta_g)$, which is able to oxidize biological targets outside the polyurethane film.

For comparison, the length l_r traveled by $O_2(^1\Delta_g)$ in an aqueous medium is 205 nm for typical values of $\tau_\Delta = 3.5$ μs and $D(O_2) = 2\times10^{-5}$ cm^2s^{-1} in H_2O. It shows that bacteria (or other biological/chemical species) should be in close contact with surfaces for efficient photooxidation. Some post-processing of hydrophobic surfaces of polymers that may prevent close contact between the surface and target structure may lead to an efficient photooxidation [92].

3.6 Production of hydroxyl (•OH) radicals

The results of measurements of photoluminescence in the presence of terephthalic acid are depicted in **Fig. 5a**. The intensity of the peak attributed to 2-hydroxyterephthalic acid (around 425 nm) is known to be proportional to the amount of •OH radicals formed. Therefore, we can conclude that the $_{200}$γ-hCQD-PU sample had the highest production of •OH radicals, and sample $_{10}$γ-hCQD-PU the lowest (**Fig. 5a**).

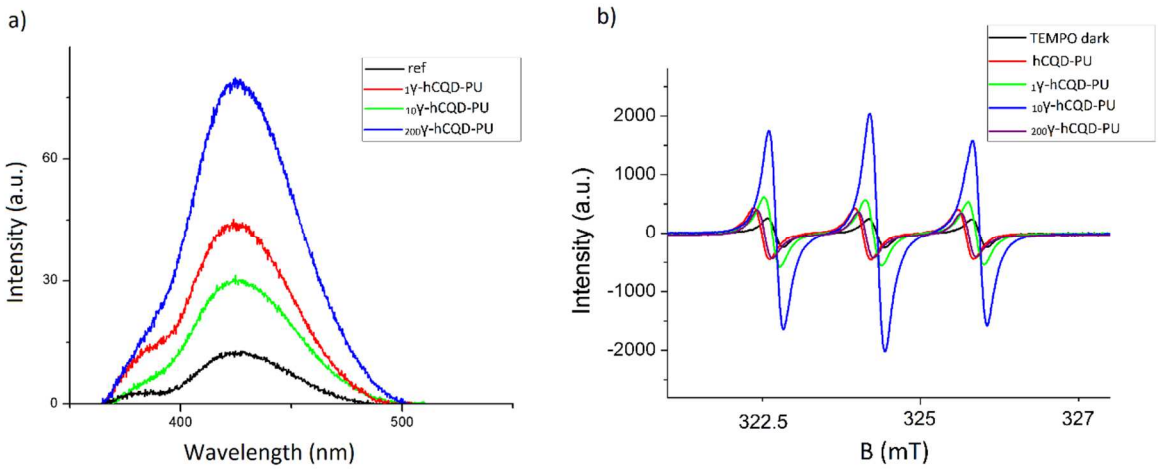

Figure 5. a) Production of •OH radicals, measured by photoluminescence, for γ-irradiated hCQD-PU nanocomposites, and b) Production of singlet oxygen measured by EPR method before and after γ-irradiation pre-treatment (from [65]).

From the obtained results (**Fig. 4**), we can conclude that the singlet oxygen lifetime was nearly the same for all the samples. However, from electron paramagnetic resonance (EPR) measurements we reported previously [65] (**Fig. 5b**), we could notice that the production of singlet oxygen was the highest for the $_{10}\gamma$-hCQD-PU sample. This is because these two techniques are quite different. EPR signal reflects only singlet oxygen which diffused to nanocomposite environment and formed 2,2,6,6-tetramethylpiperidine-1-oxyl (TEMPO). In the method presented here (**Fig. 4**), we could determine singlet oxygen production of hCQDs in the polymer matrix and its decay in both polymer matrix and its environment [93].

3.7 Determination of free radicals by EPR

The EPR measurements were conducted in order to investigate the formation of free radical species in both pure PU and hCQD-PU nanocomposites before and after gamma-irradiation treatment.

We analyzed the production of radicals using DMPO as a spin trap sensitive to several radicals [94]. Both pure PU and hCQD-PU nanocomposites showed a typical spin-adducts signal confirming the formation of free radicals **(Fig. 6a**). We studied the effect of UV light on the EPR spectra and observed the signal that corresponds to DMPO-CH_3 adduct (a_N = 15.1 G, a_H^β = 21.7 G). Ethanol is an $^{\bullet}$OH radical scavenger and its reaction with $^{\bullet}$OH, formed during irradiation in our setup, resulted in the formation of DMPO-CH_3 adduct. The concentration of DMPO-CH_3 adduct is proportional to the initial yield of $^{\bullet}$OH radicals. The EPR signal intensities are presented in **Figure 6b.** We can conclude that the sample $_{200}\gamma$-hCQD-PU had significantly higher intensity than other samples, confirming once again the highest production of $^{\bullet}$OH radicals. We can also conclude that the pure PU after the gamma-irradiation at the dose of 200 kGy did as well produce a notable amount of the free radicals, while at lower doses (1 and 10 kGy) this production dropped, compared even to the pure PU. We suppose that the gamma-irradiation of the highest dose induced the increased production of free radicals in both PU matrix and hCQDs incorporated inside.

Free radicals emerge as a result of bond scissions, and they always appear in pairs. In a liquid, the lifetimes of these various species are extremely short. They arise as a result of very fast radical-radical coupling and positive ion interactions with either electrons or negative ions. However, if a polymer is irradiated in a vitreous state, like our samples, the mobilities are considerably reduced and trapped radicals and ions are always present. The lifetimes of these species may become extremely long (weeks, months…) [60].

In carbon-based nanomaterials, gamma-irradiation induces changes mainly by Compton scattering [63]. This irradiation induces a knock-on of C atoms and the vacancies formation. But, if the material is highly defective, the saturation with defects can be achieved and the opposite process may occur – the annealing and repairing of defects in the crystalline structure. Thus, at low doses, the gamma irradiation produced defects in CQDs structure, while at a dose of 200 kGy the crystallinity of CQDs inside PU was improved by the annealing effect of gamma irradiation. Namely, annealing is occurring when the transfer of energy in the collision of gamma photon and C atoms is lower than the displacement threshold energy, thus the energy excess is eliminated as thermal energy. This causes the local temperature to increase and consequently the annealing. This effect was detected in XPS spectra, where the at% of sp^2 C was increasing from 28.9 to 49.2 %, at 0 to 200 kGy, respectively, while consequently, the at% of sp^3 C decreased.

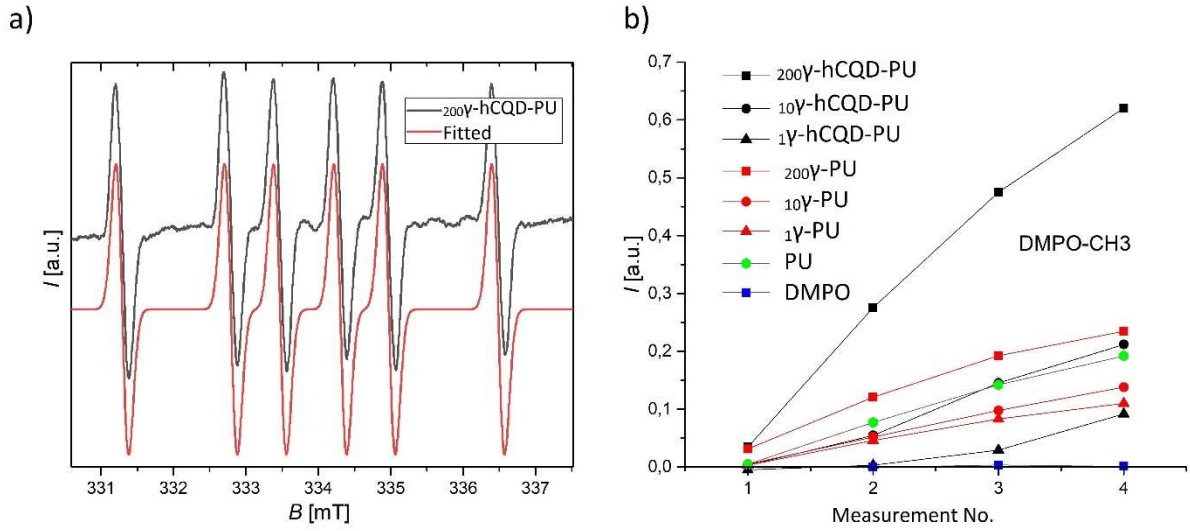

Figure 6. a) EPR spectrum (typical) of $_{200}$γ-hCQD-PU – black line, Fitted EPR spectrum – red line, obtained values a_N = 1.505 mT, a_H^β = 2.178 mT. b) EPR signal intensities of pure PU, PU after gamma irradiation, and hCQD-PU nanocomposites after gamma-irradiation. Measurement No: 1 – 0.5 min, 2 – 2 min, 3 – 3.5 min, and 4 – 5 min.

3.8 Antimicrobial activity of γ-irradiated hCQD-PU samples under blue light irradiation

Antibacterial tests were performed on two microbe strains: *S. aureus* and *E. coli,* according to ISO 22196 standard. In the first experiment, when the irradiation time was 15 min, the starting concentration of bacteria was 10^6 CFU/cm^2 for *S. aureus* and 2 ×10^6 CFU/cm^2 for *E. coli*. In the second experiment, we lowered the irradiation time to 5 min and

the starting concentration of bacteria was 9.4×10^6 CFU/cm^2 for *S. aureus* and 1.3×10^7 CFU/cm^2 for *E. coli*. Before pre-treatment with γ irradiation, hCQD-PU exhibited significant antibacterial properties after 60 min of exposure to blue light [66]. However, in our experiment, good antibacterial activity was exhibited after 15 min, already. The results of antibacterial testing are summarized in **Table S1** and presented in **Figs. 7** and **S5**. The number of viable bacteria recovered per cm^2 per test specimen (N) and antibacterial activity (R) is displayed in **Table S1** for each sample.

Data presented in **Fig. 7** and **Fig. S5** indicate that gamma-irradiated hCQD-PU nanocomposites have higher efficacy toward both types of tested bacteria strains compared to pure PU and hCQD-PU before gamma irradiation [66], but also toward gamma-pretreated pure PU. The PU or the blue light alone had no toxic effects on bacteria [66], which is in accordance with the results of Barneck et al., claiming that the light of the wavelength longer than 405 nm has no toxic effect on bacteria [95].

From antibacterial tests, we can conclude that the $_{200}$γ-hCQD-PU had the highest antibacterial efficiency (100%) towards both strains, after only 15 min exposure to the blue light. This is due to the increased production of ROS after the high dose of gamma irradiation, but also due to the increase in surface roughness of the $_{200}$γ-hCQD-PU sample. ROS targets the genetic material of the microorganisms, such as DNA, which finally results in microbial cell death [96]. Although the singlet oxygen generation was the same in all the nanocomposite samples, the production of •OH radicals was the highest for the $_{200}$γ-hCQD-PU, which resulted in higher antibacterial efficiency. Cho et al. proved that the role of •OH radicals in the inactivation of *E. coli* was dominant among all the ROS [97]. However, the lifetime of •OH radicals is very short [98], so only those hCQDs on the surface of PU could participate in the antibacterial effect. This is in accordance with our antibacterial results showing (**Table S1**) that the inactivation of *E. coli* (R ($_{200}$γ-hCQD-PU) > R ($_{1}$γ-hCQD-PU) > R ($_{10}$γ-hCQD-PU)) exhibited the same trend as the production of •OH radicals (**Fig. 5b**). Additionally, the antibacterial activity was higher towards Gram-negative bacteria, probably because *S. aureus* has the ability to adapt to oxidative stress by forming small colony variants that are resistant to ROS [99]. From the second experiment when the time was lowered to 5 min, we could notice the antibacterial efficiency only for the $_{200}$γ-hCQD-PU sample (38% for *S. aureus* and 59% for *E. coli*).

Upon exposure to the blue light, the hCQDs encapsulated closer to the surface of the polymer matrix produce ROS, that are diffusing from the polymer matrix and destroying the bacteria cell membranes. After gamma irradiation, the production of ROS increased, but also the surface roughness and wetting properties of samples have changed. Samples with higher surface roughness exhibit also bigger diffusion channels [93]. We suppose that these changes allowed the increase of the diffusion of ROS through the polymer matrix and a closer exposure of microbes to ROS. Unlike other photosensitizers, which very often need to be triggered by UV light, hCQDs are resistant to photobleaching and produce ROS whenever they are exposed to blue light. This property makes gamma-irradiated hCQD-PU nanocomposites a very promising antibacterial material.

Pure PU after gamma irradiation also exhibited certain antibacterial activity, which is due to the free-radicals formation in polyurethane after gamma-irradiation. However, it was insufficient and it was not dose-dependent, compared to the significant antibacterial activity that was exhibited in hCQD-PU nanocomposites after the gamma pre-treatment, confirming that the main antibacterial effectiveness originates from the hCQDs encapsulated inside the PU matrix.

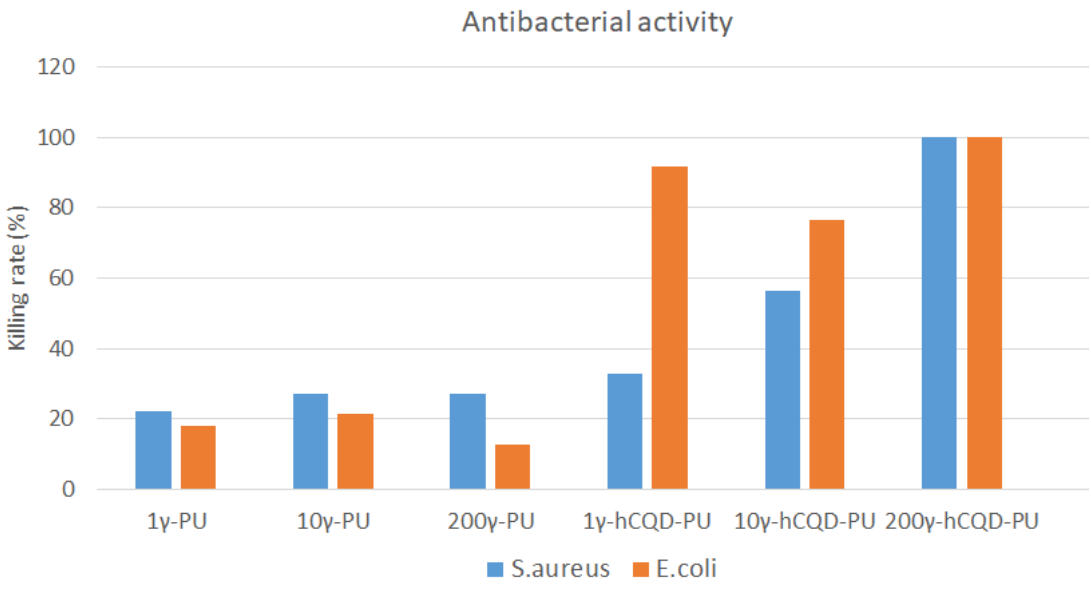

Figure 7. Antibacterial activity of γ-irradiated samples after 15 min of exposure to the blue lamp (15 W).

3.9 Cytotoxicity study of released extracts

One of the most important requirements of any material with application in medicine or biotechnology is low toxicity. The viability studies of pure PU, gamma-irradiated pure PU (PU-200), and γ-irradiated hCQD-PU samples, were conducted over two different cell lines HeLa and U-87 MG. **Figure 8** depicts the cell viability of individual samples in various extract concentrations. As can be seen from the figure, none of the tested samples revealed cytotoxicity toward HeLa cells, regardless of the extract concentration (**Fig. 8a**). However, for U-87 MG cells, only the $_{200}$γ-hCQD-PU sample exhibited mild or moderate toxicity, and only when extract concentrations were 75 and 100%, respectively (**Fig. 8b**). It should be noted that U-87 MG cells are generally more sensitive than HeLa cells. These results are consistent with the results previously published by our group [66].

Additionally, these results indicate that the pure PU after gamma pre-treatment ($_{200}$γ-PU) did not exhibit cytotoxicity to any type of cells, confirming that the toxicity towards bacteria originates from the photodynamic effect of the incorporated hCQDs.

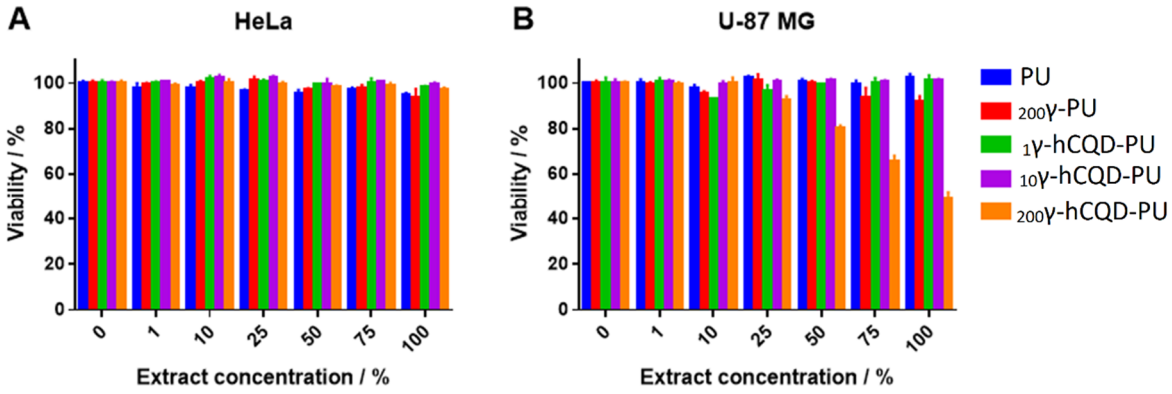

Figure 8. Cell viability of different samples in various extract concentrations towards a) HeLa cells, and b) U-87 MG cells.

3.10 Cell proliferation and growth

For any bio-interface, another important characteristic is the ability of cells to attach, grow and proliferate. Cell adhesion to a surface is a very complex process that includes three phases: protein adsorption (it takes place after the material surface comes into contact with biological fluids), the attachment, and the adhesion phase. Similarly, as in the bacteria attachment, the surface roughness is also very important in the cell attachment mechanism [100].

Figure 9 displays the viable fraction of adherent cells that can grow directly on different surfaces. Treated polystyrene (PS) surfaces (Nunclon™ Delta) were used as a reference. The results showed that both cell lines also grow similarly on glass slides under the same conditions. Besides that, only a fraction of cells were able to adhere and proliferate on pure polyurethane surfaces during 48 h (around 60% and 20% for HeLa and U-87 MG, respectively). For all other γ-pretreated surfaces with or without hCQDs, only 30% and 20% of HeLa and U-87 MG cells were able to grow on these surfaces, respectively. In order to confirm these results, the experiments were repeated and the cells were fixed and visualized under fluorescence microscopy (**Fig. S6** and **S7**). In a previous study published by our group, it was found that hCQD-PU nanocomposites were resistant against the attachment and proliferation of *eukaryotic* cells [66], and in this study, we obtained similar results, regardless of the gamma pre-treatment used.

The fluorescence microscopy images confirmed that even on the pure PU, cells were not able to grow homogenously, forming clusters and spheroids (**Fig. S6** and **S7**).

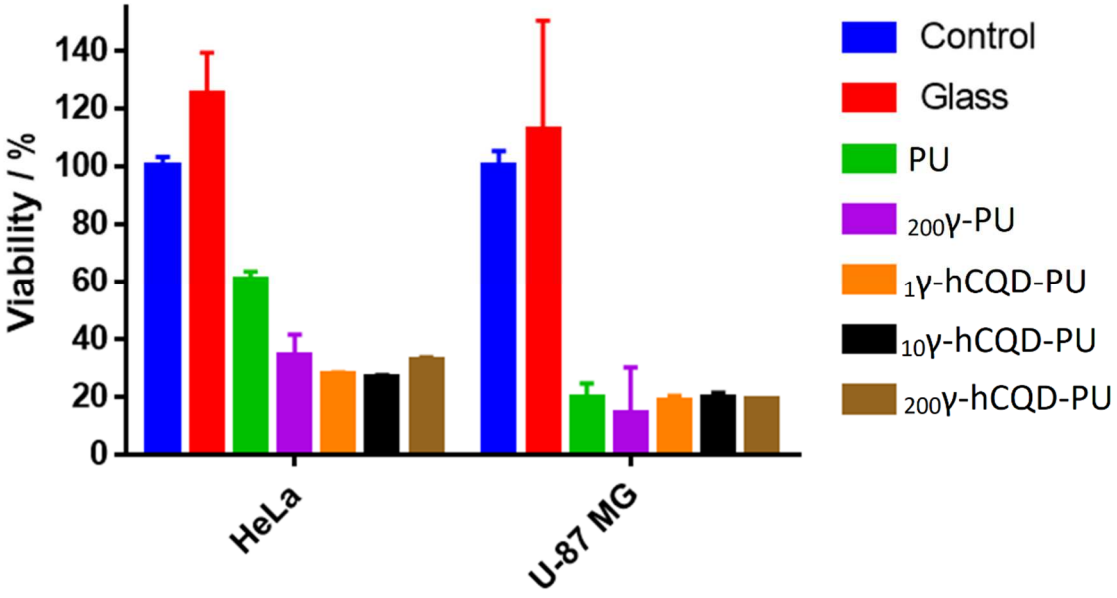

Figure 9. The viability after 48 h of HeLa and U-87 MG cells directly seeded on Polystyrene (PS, control) as a reference; glass; pure polyurethane (PU); polyurethane irradiated by 200 kGy ($_{200}$γ-PU), and $_{1}$γ-hCQD-PU, $_{10}$γ-hCQD-PU, and $_{200}$γ-hCQD-PU samples.

From these results, we can conclude that gamma irradiation pre-treatment, by increasing the production of ROS significantly, improved material's toxicity towards *prokaryotic* cells, while it did not influence the toxicity towards *eukaryotic* cells.

Depending on the application of a bio-interface, the cell attachment can be either desirable or undesirable property. When designing bone implants, for example, it is desirable for cells to easily attach and grow on the surface of an implant. On the contrary, biomaterials that have to interact with blood are required not to be adherent to cells [101].

4. Conclusion

In this work, we explored the influence of gamma irradiation at different doses (1, 10, and 200 kGy) on the physical, chemical, and antibacterial properties of hCQD-PU nanocomposites. The results showed that γ-irradiation pre-treatment of hCQD-PU nanocomposites led to changes in the surface roughness and contact angle. Also, we proved that gamma irradiation improved the ability of composites to produce oxygen-containing free radical species and reduced their capacity to quench free radicals. The production of •OH radicals was the highest in $_{200}$γ-hCQD-PU. Additionally, the percentage of sp^2 groups significantly increased with the increase of the irradiation dose. We may therefore presume that gamma irradiation had a major effect on nanocomposites' chemical properties. Consequently, it significantly improved the antibacterial activity of gamma-irradiated nanocomposites, compared to the same nanocomposite before the pre-treatment [66]. Although the largest lowering in RSA values was detected for $_{10}$γ-hCQD-PU nanocomposite, as well as the highest singlet oxygen production upon illumination, this sample did not demonstrate the highest antibacterial activity. The $_{200}$γ-hCQD-PU nanocomposite exhibited the highest antibacterial activity, which is a consequence of the highest production of •OH radicals, the largest surface roughness, and low RSA value. The sample $_{200}$γ-hCQD-PU exhibited excellent antibacterial properties after 15 min of exposure to the blue lamp and significant antibacterial activity after only 5 min. Additionally, the cell proliferation tests showed that all the samples had low cell proliferation or growth, regardless of the irradiation dose. This is an important property in the design of certain bio-interfaces where cell adhesion can induce pathological effects. Viability tests proved that only the $_{200}$γ-hCQD-PU sample exhibited certain cytotoxicity towards the U87MG cell line, but only when the extract concentration was 75 and 100%, while none of the samples displayed toxic effects towards HeLa cells. Fast and efficient antibacterial activity (that is triggered by visible light) and low toxicity, might make gamma-irradiated hCQD-PU nanocomposites excellent candidates for various antibacterial surfaces and bio-interfaces.

Conflicts of interest

There are no conflicts of interest to declare.

Acknowledgments: The research was funded by the Ministry of Education, Science and Technological Development of the Republic of Serbia (Grant No. 451-03-9/2021-14/200017).

References

[1] S.B. Levy, M. Bonnie, Antibacterial resistance worldwide: Causes, challenges and responses, Nat. Med. 10 (2004) S122–S129. doi:10.1038/nm1145.

[2] B. Spellberg, R. Guidos, D. Gilbert, J. Bradley, H.W. Boucher, W.M. Scheld, J.G. Bartlett, J. Edwards, The Epidemic of Antibiotic-Resistant Infections: A Call to Action for the Medical Community from the Infectious Diseases Society of America, Clin. Infect. Dis. 46 (2008) 155–164. doi:10.1086/524891.

[3] J.W. Costerton, P.S. Stewart, E.P. Greenberg, Bacterial biofilms: A common cause of persistent infections, Science . 284 (1999) 1318–1322. doi:10.1126/science.284.5418.1318.

[4] P. Zarb, B. Coignard, J. Griskeviciene, A. Muller, V. Vankerckhoven, K. Weist, M.M. Goossens, S. Vaerenberg, S. Hopkins, B. Catry, D.L. Monnet, H. Goossens, C. Suetens, The european centre for disease prevention and control (ECDC) pilot point prevalence survey of healthcare-associated infections and antimicrobial use, Eurosurveillance. 17 (2012) 1–16. doi:10.2807/ese.17.46.20316-en.

[5] M. Cloutier, D. Mantovani, F. Rosei, Antibacterial Coatings: Challenges, Perspectives, and Opportunities, Trends Biotechnol. 33 (2015) 637–652. doi:10.1016/j.tibtech.2015.09.002.

[6] A.Y. Peleg, D.C. Hooper, Hospital-acquired infections due to gram-negative bacteria, N. Engl. J. Med. 362 (2010) 1804–1813. doi:10.1056/NEJMra0904124.

[7] B. Allegranzi, S.B. Nejad, C. Combescure, W. Graafmans, H. Attar, L. Donaldson, D. Pittet, Burden of endemic health-care-associated infection in developing countries: Systematic review and meta-analysis, Lancet. 377 (2011) 228–241. doi:10.1016/S0140-6736(10)61458-4.

[8] J. Hasan, R.J. Crawford, E.P. Ivanova, Antibacterial surfaces: The quest for a new generation of biomaterials, Trends Biotechnol. 31 (2013) 295–304. doi:10.1016/j.tibtech.2013.01.017.

[9] A. Elbourne, R.J. Crawford, E.P. Ivanova, Nano-structured antimicrobial surfaces: From nature to synthetic analogues, J. Colloid Interface Sci. 508 (2017) 603–616. doi:10.1016/j.jcis.2017.07.021.

[10] I. Armentano, C.R. Arciola, E. Fortunati, D. Ferrari, S. Mattioli, C.F. Amoroso, J. Rizzo, J.M. Kenny, M. Imbriani, L. Visai, The Interaction of Bacteria with Engineered Nanostructured Polymeric Materials: A Review, (2014). doi:10.1155/2014/410423.

[11] X. Zhang, L. Wang, E. Levänen, Superhydrophobic surfaces for the reduction of bacterial adhesion, RSC Adv. 3 (2013) 12003–12020. doi:10.1039/c3ra40497h.

[12] M. Sile-Yuksel, B. Tas, D.Y. Koseoglu-Imer, I. Koyuncu, Effect of silver nanoparticle (AgNP) location in nanocomposite membrane matrix fabricated with different polymer type on antibacterial mechanism, Desalination. 347 (2014) 120–130. doi:10.1016/J.DESAL.2014.05.022.

[13] A. Sirelkhatim, S. Mahmud, A. Seeni, N. Haida, M. Kaus, L. Chuo, A.• Siti, K. Mohd Bakhori, H. Hasan, D. Mohamad, A. Sirelkhatim, Á.S. Mahmud, Á.L.C. Ann, Á.S.K.M. Bakhori, A. Seeni, N.H.M. Kaus, H. Hasan, D. Mohamad, Review on Zinc Oxide Nanoparticles: Antibacterial Activity and Toxicity Mechanism, Nano-Micro Lett. 7 (2015) 219–242. doi:10.1007/s40820-015-0040-x.

[14] O. Carp, C.L. Huisman, A. Reller, Photoinduced reactivity of titanium dioxide, Prog. Solid State Chem. 32 (2004) 33–177. doi:10.1016/J.PROGSOLIDSTCHEM.2004.08.001.

[15] Y. Cui, Y. Zhao, Y. Tian, W. Zhang, X. Lü, X. Jiang, The molecular mechanism of action of bactericidal gold nanoparticles on Escherichia coli, Biomaterials. 33 (2012) 2327–2333. doi:10.1016/j.biomaterials.2011.11.057.

[16] S. Perni, C. Piccirillo, J. Pratten, P. Prokopovich, W. Chrzanowski, I.P. Parkin, M. Wilson, The antimicrobial properties of light-activated polymers containing methylene blue and gold nanoparticles, Biomaterials. 30 (2009) 89–93. doi:10.1016/j.biomaterials.2008.09.020.

[17] J.C. Tiller, C.J. Liao, K. Lewis, A.M. Klibanov, Designing surfaces that kill bacteria on contact, Proc. Natl. Acad. Sci. U. S. A. 98 (2001) 5981–5985. doi:10.1073/pnas.111143098.

[18] J. Song, J. Jang, Antimicrobial polymer nanostructures: Synthetic route, mechanism of action and perspective, Adv. Colloid Interface Sci. 203 (2014) 37–50. doi:10.1016/j.cis.2013.11.007.

[19] P.A. Norowski, J.D. Bumgardner, Biomaterial and antibiotic strategies for peri-implantitis, J. Biomed. Mater. Res. - Part B Appl. Biomater. 88 (2009) 530–543. doi:10.1002/jbm.b.31152.

[20] G. Gao, D. Lange, K. Hilpert, J. Kindrachuk, Y. Zou, J.T.J. Cheng, M. Kazemzadeh-Narbat, K. Yu, R. Wang, S.K. Straus, D.E. Brooks, B.H. Chew, R.E.W. Hancock, J.N. Kizhakkedathu, The biocompatibility and biofilm resistance of implant coatings based on hydrophilic polymer brushes conjugated with antimicrobial peptides, Biomaterials. 32 (2011) 3899–3909. doi:10.1016/j.biomaterials.2011.02.013.

[21] M. Cho, H. Chung, W. Choi, J. Yoon, E. Marti, E. Variatza, J.L. Balcazar, J. Jiang, C. Zhang, G.M. Zeng, J.L. Gong, Y.N. Chang, B. Song, C.H. Deng, H.Y. Liu, K. Wang, X. Lin, G. Jiang, J.Z.J. Liu, L. Jiang, C.M. Doherty, A.J. Hill, T. Xu, H. Wang, S. Lin, R. Huang, Y. Cheng, J.Z.J. Liu, B.L.T. Lau, M.R. Wiesner, J. Lalley, D.D. Dionysiou, R.S. Varma, S. Shankara, D.J. Yang, M.N. Nadagouda, Silver nanoparticle-alginate composite beads for point-of-use drinking water disinfection, Trends Microbiol. 22 (2014) 25–29. doi:10.1016/j.coche.2013.09.004.

[22] Q. Li, S. Mahendra, D.Y. Lyon, L. Brunet, M. V. Liga, D. Li, P.J.J. Alvarez, Antimicrobial nanomaterials for water disinfection and microbial control: Potential applications and implications, Water Res. 42 (2008) 4591–4602. doi:10.1016/j.watres.2008.08.015.

[23] L.-E. Shi, L. Xing, B. Hou, H. Ge, X. Guo, Z. Tang, Inorganic nano mental oxides used as anti-microorganism agents for pathogen control, Curr. Res. Technol. Educ. Top. Appl. Microbiol. Microb. Biotechnol. (2010) 361–368. http://www.formatex.info/microbiology2/361-368.pdf (accessed December 11, 2018).

[24] M.J. Hajipour, K.M. Fromm, A. Akbar Ashkarran, D. Jimenez de Aberasturi, I.R. de Larramendi, T. Rojo, V. Serpooshan, W.J. Parak, M. Mahmoudi, Antibacterial properties of nanoparticles, Trends Biotechnol. 30 (2012) 499–511. doi:10.1016/J.TIBTECH.2012.06.004.

[25] I. Anghel, A.M. Grumezescu, A.M. Holban, A. Ficai, A.G. Anghel, M.C. Chifiriuc, Biohybrid nanostructured iron oxide nanoparticles and Satureja hortensis to prevent fungal biofilm development, Int. J. Mol. Sci. 14 (2013) 18110–18123. doi:10.3390/ijms140918110.

[26] Z.M. Xiu, J. Ma, P.J.J. Alvarez, Differential effect of common ligands and molecular oxygen on antimicrobial activity of silver nanoparticles versus silver ions, Environ. Sci. Technol. 45 (2011) 9003–9008. doi:10.1021/es201918f.

[27] S.Y. Liau, D.C. Read, W.J. Pugh, J.R. Furr, A.D. Russell, Interaction of silver nitrate with readily identifiable groups: relationship to the antibacterialaction of silver ions, Lett. Appl. Microbiol. 25 (1997) 279–283. doi:10.1046/j.1472-765X.1997.00219.x.

[28] J.O.K. Q.L. Feng, J. Wu, G.Q. Chen, F.Z. Cui, T.M. Kim, A mechanistic study of the antibacterial effect of silver ions on E. coli and S. aureus, J. Biomed. Mater. Res. 52 (2000) 662–668. doi:doi.org/10.1002/1097-4636(20001215)52:4<662::AID-JBM10>3.0.CO;2-3.

[29] S.K. Das, A.R. Das, A.K. Guha, Gold Nanoparticles: Microbial Synthesis and Application in Water Hygiene Management, Langmuir. 25 (2009) 8192–8199. doi:10.1021/la900585p.

[30] Ramdayal, K. Balasubramanian, Antibacterial application of polyvinylalcohol-nanogold composite membranes, Colloids Surf A Physicochem. Eng. Asp. 455 (2014) 174–178. doi:10.1016/j.colsurfa.2014.04.050.

[31] W. Jiang, H. Mashayekhi, B. Xing, Bacterial toxicity comparison between nano- and micro-scaled oxide particles, Environ. Pollut. 157 (2009) 1619–1625. doi:10.1016/J.ENVPOL.2008.12.025.

[32] T. Matsunaga, R. Tomoda, T. Nakajima, N. Nakamura, T. Komine, Continuous-sterilization system that uses photosemiconductor powders., Appl. Environ. Microbiol. 54 (1988) 1330–3. http://www.ncbi.nlm.nih.gov/pubmed/3046487 (accessed December 5, 2018).

[33] K.P. Kühn, I.F. Chaberny, K. Massholder, M. Stickler, V.W. Benz, H.-G. Sonntag, L. Erdinger, Disinfection of surfaces by photocatalytic oxidation with titanium dioxide and UVA light, Chemosphere. 53 (2003) 71–77. doi:10.1016/S0045-6535(03)00362-X.

[34] P.K. Stoimenov, R.L. Klinger, G.L. Marchin, K.J. Klabunde, Metal oxide nanoparticles as bactericidal agents, Langmuir. 18 (2002) 6679–6686. doi:10.1021/la0202374.

[35] M. Heinlaan, A. Ivask, I. Blinova, H.-C. Dubourguier, A. Kahru, Toxicity of nanosized and bulk ZnO, CuO and TiO2 to bacteria Vibrio fischeri and crustaceans Daphnia magna and Thamnocephalus platyurus, Chemosphere. 71 (2008) 1308–1316. doi:10.1016/J.CHEMOSPHERE.2007.11.047.

[36] S. Szunerits, R. Boukherroub, Antibacterial activity of graphene-based materials, J. Mater. Chem. B. 4 (2016) 6892–6912. doi:10.1039/c6tb01647b.

[37] M. Rai, A. Yadav, A. Gade, Silver nanoparticles as a new generation of antimicrobials, Biotechnol. Adv. 27 (2009) 76–83. doi:10.1016/j.biotechadv.2008.09.002.

[38] H.J. Johnston, G. Hutchison, F.M. Christensen, S. Peters, S. Hankin, V. Stone, A review of the in vivo and in vitro toxicity of silver and gold particulates: Particle attributes and biological mechanisms responsible for the observed toxicity, Crit. Rev. Toxicol. 40 (2010) 328–346. doi:10.3109/10408440903453074.

[39] S.Y. Lim, W. Shen, Z. Gao, Carbon quantum dots and their applications., Chem. Soc. Rev. 44 (2015) 362–81. doi:10.1039/c4cs00269e.

[40] H. Li, Z. Kang, Y. Liu, S.-T. Lee, Carbon nanodots: synthesis, properties and applications, J. Mater. Chem. 22 (2012) 24230. doi:10.1039/c2jm34690g.

[41] S.N. Baker, G.A. Baker, Luminescent Carbon Nanodots: Emergent Nanolights, Angew. Chem. Int. Ed. 49 (2010) 6726–6744. doi:10.1002/anie.200906623.

[42] Z. Gao, G. Shen, X. Zhao, N. Dong, P. Jia, J. Wu, D. Cui, Y. Zhang, Y. Wang, Carbon dots: A safe nanoscale substance for the immunologic system of mice, Nanoscale Res. Lett. 8 (2013) 1–8. doi:10.1186/1556-276X-8-276.

[43] S.T. Yang, X. Wang, H. Wang, F. Lu, P.G. Luo, L. Cao, M.J. Meziani, J.H. Liu, Y. Liu, M. Chen, Y. Huang, Y.P. Sun, Carbon dots as nontoxic and high-performance fluorescence imaging agents, J. Phys. Chem. C. 113 (2009) 18110–18114. doi:10.1021/jp9085969.

[44] P. Devi, S. Saini, K.-H.H. Kim, The advanced role of carbon quantum dots in nanomedical applications, 2019. doi:10.1016/j.bios.2019.02.059.

[45] D.E.J.G.J. Dolmans, D. Fukumura, R.K. Jain, Photodynamic therapy for cancer, Nat. Rev. Cancer. 3 (2003) 380–387. doi:10.1038/nrc1071.

[46] M. Athar, H. Mukhtar, D.R. Bickers, Differential role of reactive oxygen intermediates in photofrin-I- and photofrin-II-mediated photoenhancement of lipid peroxidation in epidermal microsomal membranes, J. Invest. Dermatol. 90 (1988) 652–657. doi:10.1111/1523-1747.ep12560814.

[47] R. Knoblauch, C.D. Geddes, Carbon Nanodots in Photodynamic Antimicrobial Therapy: A Review, Materials (Basel). 13 (2020) 4004. doi:10.3390/ma13184004.

[48] X. Nie, C. Jiang, S. Wu, W. Chen, P. Lv, Q. Wang, J. Liu, C. Narh, X. Cao, R.A. Ghiladi, Q. Wei, Carbon quantum dots: A bright future as photosensitizers for in vitro antibacterial photodynamic inactivation, J. Photochem. Photobiol. B Biol. 206 (2020) 111864. doi:10.1016/j.jphotobiol.2020.111864.

[49] N.K. Stanković, M. Bodik, P. Šiffalovič, M. Kotlar, M. Mičušik, Z. Špitalsky, M. Danko, D.D. Milivojević, A. Kleinova, P. Kubat, Z. Capakova, P. Humpoliček, M. Lehocky, B.M. Todorović Marković, Z.M. Marković, Antibacterial and Antibiofouling Properties of Light Triggered Fluorescent Hydrophobic Carbon Quantum Dots Langmuir-Blodgett Thin Films, ACS Sustain. Chem. Eng. 6 (2018) 4154–4163. doi:10.1021/acssuschemeng.7b04566.

[50] R. Knoblauch, A. Harvey, E. Ra, K.M. Greenberg, J. Lau, E. Hawkins, C.D. Geddes, Antimicrobial carbon nanodots: Photodynamic inactivation and dark antimicrobial effects on bacteria by brominated carbon nanodots, Nanoscale. 13 (2021) 85–99. doi:10.1039/d0nr06842j.

[51] F. Zhao, W. Gu, J. Zhou, Q. Liu, Y. Chong, Solar-excited graphene quantum dots for bacterial inactivation via generation of reactive oxygen species, J. Environ. Sci. Heal. - Part C Environ. Carcinog. Ecotoxicol. Rev. 37 (2019) 67–80. doi:10.1080/10590501.2019.1591701.

[52] J. Zhang, X. Liu, X. Wang, L. Mu, M. Yuan, B. Liu, H. Shi, Carbon dots-decorated Na 2 W 4 O 13 composite with WO 3 for highly efficient photocatalytic antibacterial activity, J. Hazard. Mater. 359 (2018) 1–8. doi:10.1016/j.jhazmat.2018.06.072.

[53] J. Zhang, X. Lu, D. Tang, S. Wu, X. Hou, J. Liu, P. Wu, Phosphorescent Carbon Dots for Highly Efficient Oxygen Photosensitization and as Photo-oxidative Nanozymes, ACS Appl. Mater. Interfaces. 10 (2018) 40808–40814. doi:10.1021/acsami.8b15318.

[54] H. Shintani, H. Kikuchi, A. Nakamura, Effects of gamma-ray irradiation on the change of characteristics of polyurethane, Polym. Degrad. Stab. 32 (1991) 17–30. doi:10.1016/0141-3910(91)90059-Z.

[55] L. Montanari, M. Costantini, E.C. Signoretti, L. Valvo, M. Santucci, M. Bartolomei, P. Fattibene, S. Onori, A. Faucitano, B. Conti, I. Genta, Gamma irradiation effects on poly(DL-lactictide-co-glycolide) microspheres, J. Control. Release. 56 (1998) 219–229. doi:10.1016/S0168-3659(98)00082-0.

[56] R. Brígido Diego, M. Salmerón Sánchez, J.L. Gómez Ribelles, M. Monleón Pradas, Effect of γ-irradiation on the structure of poly(ethyl acrylate-co-hydroxyethyl methacrylate) copolymer networks for biomedical applications, J. Mater. Sci. Mater. Med. 18 (2007) 693–698. doi:10.1007/s10856-006-0008-y.

[57] A. Buttafava, G. Consolati, L. Di Landro, M. Mariani, γ-irradiation effects on

polyethylene terephthalate studied by positron annihilation lifetime spectroscopy, Polymer (Guildf). 43 (2002) 7477–7481. doi:10.1016/S0032-3861(02)00708-5.

[58] H. Kausch, Radiation effects on polymers for biological use: Preface, Springer Berlin Heidelberg, Berlin, Heidelberg, 2003. doi:10.1007/3-540-45668-6.

[59] D.J.T. Hill, A.K. Whittaker, Radiation Chemistry of Polymers, in: Encycl. Polym. Sci. Technol., John Wiley & Sons, Inc., Hoboken, NJ, USA, 2004. doi:10.1002/0471440264.pst488.

[60] A. Chapiro, Chemical modifications in irradiated polymers, Nucl. Inst. Methods Phys. Res. B. 32 (1988) 111–114. doi:10.1016/0168-583X(88)90191-7.

[61] A. Ashfaq, M.C. Clochard, X. Coqueret, C. Dispenza, M.S. Driscoll, P. Ulański, M. Al-Sheikhly, Polymerization reactions and modifications of polymers by ionizing radiation, Polymers (Basel). 12 (2020) 1–67. doi:10.3390/polym12122877.

[62] S.L. Cooke, A.R. Whittington, Investigation into Polyurethane at Varying Dose Rates of Ionizing Radiation for Clinical Application, J. Chem. 2018 (2018). doi:10.1155/2018/7312147.

[63] M.M. Ghobashy, Z.I. Abdeen, Influence of Gamma Irradiation on the Change of the Characterization of Elastomeric Polyurethane, Adv. Sci. Eng. Med. 8 (2016) 736–739. doi:10.1166/asem.2016.1908.

[64] S.P. Jovanović, Z. Syrgiannis, Z.M. Marković, A. Bonasera, D.P. Kepić, M.D. Budimir, D.D. Milivojević, V.D. Spasojević, M.D. Dramićanin, V.B. Pavlović, B.M. Todorović Marković, Modification of Structural and Luminescence Properties of Graphene Quantum Dots by Gamma Irradiation and Their Application in a Photodynamic Therapy, ACS Appl. Mater. Interfaces. 7 (2015). doi:10.1021/acsami.5b08226.

[65] M. Budimir, Z. Marković, D. Jovanović, M. Vujisić, M. Mičušík, M. Danko, A. Kleinová, H. Švajdlenková, Z. Špitalský, B.T. Marković, Gamma ray assisted modification of carbon quantum dot/polyurethane nanocomposites: Structural, mechanical and photocatalytic study, RSC Adv. 9 (2019) 6278–6286. doi:10.1039/c9ra00500e.

[66] M. Kováčová, Z.M. Marković, P. Humpolíček, M. Mičušík, H. Švajdlenková, A. Kleinová, M. Danko, P. Kubát, J. Vajďák, Z. Capáková, M. Lehocký, L. Münster, B.M. Todorović Marković, Z. Špitalský, Carbon Quantum Dots Modified Polyurethane Nanocomposite as Effective Photocatalytic and Antibacterial Agents, ACS Biomater. Sci. Eng. 4 (2018) 3983–3993. doi:10.1021/acsbiomaterials.8b00582.

[67] D. Nečas, P. Klapetek, Gwyddion: an open-source software for SPM data analysis, Open Phys. 10 (2012) 181–188. doi:10.2478/s11534-011-0096-2.

[68] V. Ruiz, L. Yate, I. García, G. Cabanero, H.-J.J. Grande, Tuning the antioxidant activity of graphene quantum dots: Protective nanomaterials against dye decoloration, Carbon . 116 (2017) 366–374. https://www.sciencedirect.com/science/article/pii/S0008622317301008 (accessed October 2, 2019).

[69] K.I. Ishibashi, A. Fujishima, T. Watanabe, K. Hashimoto, Detection of active oxidative species in TiO2 photocatalysis using the fluorescence technique, Electrochem. Commun. 2 (2000) 207–210. doi:10.1016/S1388-2481(00)00006-0.

[70] ISO, Measurement of antibacterial activity on plastics and other non-porous surfaces, Norma ISO 22196. (2011). doi:10.1017/CBO9781107415324.004.

[71] R.L. Clough, K.T. Gillen, G.M. Malone, J.S. Wallace, Color formation in irradiated polymers, in: Radiat. Phys. Chem., Pergamon Press Inc, 1996: pp. 583–594. doi:10.1016/0969-806X(96)00075-8.

[72] R.L. Clough, G.M. Malone, K.T. Gillen, J.S. Wallace, M.B. Sinclair, Discoloration and subsequent recovery of optical polymers exposed to ionizing radiation, Polym. Degrad. Stab. 49 (1995) 305–313. doi:10.1016/0141-3910(95)87013-X.

[73] J.S. Wallace, M.B. Sinclair, K.T. Gillen, R.L. Clough, Color center annealing in γ - irradiated polystyrene, under vacuum and air atmospheres, Radiat. Phys. Chem. 41 (1993) 85–100. doi:10.1016/0969-806X(93)90045-V.

[74] S.H. Al-Harthi, M. Elzain, M. Al-Barwani, A. Kora'a, T. Hysen, M.T.Z. Myint, M.R. Anantharaman, Unusual surface and edge morphologies, sp2 to sp3 hybridized transformation and electronic damage after Ar+ ion irradiation of few-layer graphene surfaces., Nanoscale Res. Lett. 7 (2012) 466. doi:10.1186/1556-276X-7-466.

[75] S.P. Jovanović, Z.M. Marković, D.N. Kleut, N.Z. Romević, V.S. Trajković, M.D. Dramićanin, B.M. Todorović Marković, A novel method for the functionalization of γ-irradiated single wall carbon nanotubes with DNA, Nanotechnology. 20 (2009). doi:10.1088/0957-4484/20/44/445602.

[76] R. Wang, B. Chen, D. Chen, X. Zhao, Effects of Gamma Irradiation on Organic Membrane Materials, Nucl. Technol. (2020). doi:10.1080/00295450.2020.1721406.

[77] V. Ivanov, Radiation chemistry of polymers, (1992). https://books.google.com/books?hl=sr&lr=&id=WOXRoh--PfsC&oi=fnd&pg=PR9&dq=Ivanov+VS.+Radiation+chemistry+of+polymers.+Zeist,+The+Netherlands:+VSP%3B+1992.&ots=0F3GoPHHl6&sig=qx1D815CqDLtKeO0NEFGVyx2wJY (accessed March 23, 2020).

[78] M. Goldman, L. Pruitt, Comparison of the effects of gamma radiation and low temperature hydrogen peroxide gas plasma sterilization on the molecular structure, fatigue resistance, and wear behavior of UHMWPE, J. Biomed. Mater. Res. 40 (1998) 378–384. doi:10.1002/(SICI)1097-4636(19980605)40:3<378::AID-JBM6>3.0.CO;2-C.

[79] Avantage Software, (n.d.). https://xpssimplified.com/avantage_data_system.php (accessed July 26, 2020).

[80] Y. Tamada, Y. Ikada, Effect of preadsorbed proteins on cell adhesion to polymer surfaces, J. Colloid Interface Sci. 155 (1993) 334–339. doi:10.1006/jcis.1993.1044.

[81] P. Alves, J.F.J. Coelho, J. Haack, A. Rota, A. Bruinink, M.H. Gil, Surface modification and characterization of thermoplastic polyurethane, Eur. Polym. J. (2009). doi:10.1016/j.eurpolymj.2009.02.011.

[82] D. Chvedov, A. Arnold, Effect of Surface Topography of a Rolled Sheet on Contact Angle, Ind. Eng. Chem. Res. 43 (2004) 1451–1459. doi:10.1021/ie0307131.

[83] K. Gorna, S. Gogolewski, The effect of gamma radiation on molecular stability and mechanical properties of biodegradable polyurethanes for medical applications, Polym. Degrad. Stab. 79 (2003) 465–474. doi:10.1016/S0141-3910(02)00362-2.

[84] S.R. Shin, J.Y. Liang, H. Ryu, G.S. Song, D.S. Lee, Effects of isosorbide incorporation into flexible polyurethane foams: Reversible urethane linkages and antioxidant activity, Molecules. 24 (2019). doi:10.3390/molecules24071347.

[85] B.-O. Jung, S.-J. Chung, S.B. Lee, Preparation and characterization of eugenol-grafted chitosan hydrogels and their antioxidant activities, J. Appl. Polym. Sci. 99 (2006) 3500–3506. doi:10.1002/app.22974.

[86] M. Bolgar, J. Hubball, J. Groeger, S. Meronek, Handbook for the Chemical Analysis of Plastic and Polymer Additives, CRC Press, 2007. doi:10.1201/9781420044881.

[87] S. Jovanović, S. Dorontić, D. Jovanović, G. Ciasca, M. Budimir, A. Bonasera, M. Scopelliti, O. Marković, B. Todorović Marković, Gamma irradiation of graphene quantum dots with ethylenediamine: Antioxidant for ion sensing, Ceram. Int. 46 (2020) 23611–23622. doi:10.1016/j.ceramint.2020.06.133.

[88] Y. Ruiz-Morales, O.C. Mullins, Singlet-triplet and triplet-triplet transitions of asphaltene PAHs by molecular orbital calculations, Energ. Fuel. 27 (2013) 5017–5028. doi:10.1021/ef400168a.

[89] J. Ge, M. Lan, B. Zhou, W. Liu, L. Guo, H. Wang, Q. Jia, G. Niu, X. Huang, H. Zhou, X. Meng, P. Wang, C.S. Lee, W. Zhang, X. Han, A graphene quantum dot photodynamic therapy agent with high singlet oxygen generation, Nat. Commun. 5 (2014) 1–8. doi:10.1038/ncomms5596.

[90] M. Bregnhøj, M. Westberg, F. Jensen, P. Ogilby, Chemistry, Solvent-dependent singlet oxygen lifetimes: temperature effects implicate tunneling and charge-transfer interactions, Phys. Chem. Chem. Phys. 18 (2016) 22946–22961. https://pubs.rsc.org/en/content/articlehtml/2016/cp/c6cp01635a (accessed October 22, 2019).

[91] S. Jesenská, L. Plíštil, P. Kubát, K. Lang, L. Brožová, Š. Popelka, L. Szatmáry, J. Mosinger, Antibacterial nanofiber materials activated by light, J. Biomed. Mater. Res. - Part A. 99 A (2011) 676–683. doi:10.1002/jbm.a.33218.

[92] P. Henke, H. Kozak, A. Artemenko, P. Kubát, J. Forstová, J. Mosinger, Superhydrophilic polystyrene nanofiber materials generating O 2(1Δg): Postprocessing surface modifications toward efficient antibacterial effect, ACS Appl. Mater. Interfaces. 6 (2014) 13007–13014. doi:10.1021/am502917w.

[93] Z.M. Marković, M. Kováčová, P. Humpolíček, M.D. Budimir, J. Vajďák, P. Kubát, M. Mičušík, H. Švajdlenková, M. Danko, Z. Capáková, M. Lehocký, B.M. Todorović Marković, Z. Špitalský, Antibacterial photodynamic activity of carbon quantum dots/polydimethylsiloxane nanocomposites against Staphylococcus aureus, Escherichia coli and Klebsiella pneumoniae, Photodiagnosis Photodyn. Ther. 26 (2019) 342–349. doi:10.1016/j.pdpdt.2019.04.019.

[94] Experimental Protocol, n.d. www.bruker-biospin.com (accessed October 18, 2020).

[95] M.D. Barneck, N.L.R. Rhodes, M. de la Presa, J.P. Allen, A.E. Poursaid, M.M. Nourian, M.A. Firpo, J.T. Langell, Violet 405-nm light: a novel therapeutic agent against common pathogenic bacteria, J. Surg. Res. 206 (2016) 316–324. doi:10.1016/j.jss.2016.08.006.

[96] Y. Liu, X. Zeng, X. Hu, J. Hu, X. Zhang, Two-dimensional nanomaterials for photocatalytic water disinfection: recent progress and future challenges, J. Chem. Technol. Biotechnol. 94 (2019) 22–37. doi:10.1002/jctb.5779.

[97] M. Cho, H. Chung, W. Choi, J. Yoon, Linear correlation between inactivation of E. coli and OH radical concentration in TiO2 photocatalytic disinfection, Water Res. 38 (2004) 1069–1077. http://linkinghub.elsevier.com/retrieve/pii/S004313540300602X (accessed December 5, 2018).

[98] P. Attri, Y.H. Kim, D.H. Park, J.H. Park, Y.J. Hong, H.S. Uhm, K.N. Kim, A. Fridman, E.H. Choi, Generation mechanism of hydroxyl radical species and its lifetime prediction during the plasma-initiated ultraviolet (UV) photolysis, Sci. Rep. 5 (2015). doi:10.1038/srep09332.

[99] K.L. Painter, E. Strange, J. Parkhill, K.B. Bamford, D. Armstrong-James, A.M. Edwards, Staphylococcus aureus adapts to oxidative stress by producing H2O2-resistant small-colony variants via the SOS response, Infect. Immun. 83 (2015) 1830–1844. doi:10.1128/IAI.03016-14.

[100] K. Anselme, Osteoblast adhesion on biomaterials, Biomaterials. 21 (2000) 667–681. doi:10.1016/S0142-9612(99)00242-2.

[101] A.A. Khalili, M.R. Ahmad, A Review of cell adhesion studies for biomedical and biological applications, Int. J. Mol. Sci. 16 (2015) 18149–18184. doi:10.3390/ijms160818149.